Journal of Medicinal Chemistry

Article

Synthesis, radiolabeling, and biological evaluation of (*R*)- and (*S*)-2-amino-5-[F]fluoro-2-methylpentanoic acid ((*R*)-, (*S*)-[F]FAMPe) as potential positron emission tomography tracers for brain tumors

Ahlem Bouhlel, Dong Zhou, Aixiao Li, Liya Yuan, Keith Rich, and Jon McConathy

J. Med. Chem., **Just Accepted Manuscript** • DOI: 10.1021/jm502023y • Publication Date (Web): 06 Apr 2015

Just Accepted

Journal of Medicinal Chemistry is published by the American Chemical Society. 1155 Sixteenth Street N.W., Washington, DC 20036

Synthesis, radiolabeling, and biological evaluation of (*R*)- and (*S*)-2-amino-5-[^{18}F]fluoro-2-methylpentanoic acid ((*R*)-, (*S*)-[^{18}F]FAMPe) as potential positron emission tomography tracers for brain tumors

Bouhlel, Ahlem[1]; Zhou, Dong[1]; Li, Aixiao[1]; Yuan, Liya[2]; Rich, Keith[2]; McConathy, Jonathan[1*].

[1]Department of Radiology, Washington University in Saint Louis, School of Medicine, Missouri

[2]Department of Neurosurgery, Washington University in Saint Louis, School of Medicine, Missouri.

Abstract

A novel ^{18}F-labeled α,α-disubstituted amino acid-based tracer, 2-amino-5-[^{18}F]fluoro-2-methylpentanoic acid ([^{18}F]FAMPe) has been developed for brain tumor imaging with a longer alkyl side chain than previously reported compounds to increase brain availability via system L amino acid transport. Both enantiomers of [^{18}F]FAMPe were obtained in good radiochemical yield (24-52% n= 8) and high radiochemical purity (> 99%). In vitro uptake assays in mouse DBT gliomas cells revealed that (*S*)-[^{18}F]FAMPe enters cells partly via sodium-independent system L transporters and also via other non-system A transport systems including transporters that recognize glutamine. Biodistribution and small animal PET/CT studies in the mouse DBT model of glioblastoma showed that both (*R*)- and (*S*)-[^{18}F]FAMPe have good tumor imaging properties with the (*S*)-enantiomer providing higher tumor uptake and tumor to brain ratios. Comparison of the SUVs showed that (*S*)-[^{18}F]FAMPe had higher tumor to brain ratios compared to (*S*)-[^{18}F]FET, a well-established system L substrate.

Introduction

Brain tumor imaging with the most widely used positron emission tomography (PET) tracer for oncology, the glucose analogue 2-deoxy-2-[^{18}F]fluoro-D-glucose ([^{18}F]FDG), is often difficult to interpret due to the high physiologic uptake of [^{18}F]FDG in normal brain and variable [^{18}F]FDG uptake in regions showing post-treatment effects such as radiation necrosis.[1-3] In contrast to [^{18}F]FDG, radiolabeled amino acid tracers targeting system L amino acid transporters have superior brain tumor imaging properties due to upregulation of amino acid transporters in gliomas and lower uptake in normal brain.[1, 4] These tracers complement anatomic imaging with magnetic resonance imaging (MRI) for definition of tumor margins, monitoring response to therapy, and distinguishing treatment effects from recurrent tumor. System L preferentially transports amino acids with large, neutral side chains (e.g. L-phenylalanine, L-tyrosine, L-leucine) and has four family members: LAT1, LAT2, LAT3, and LAT4. LAT1 and LAT2 are sodium-

independent and function by exchanging one intracellular amino acid for one extracellular amino acid whereas LAT3 and LAT4 mediate facilitated diffusion of substrates across membranes. System L transporters are active at the luminal side of the blood-brain barrier (BBB) which allows system L substrates to reach the entire tumor volume even when the BBB is not disrupted. A number of well-established PET tracers targeting system L transport have been used for human brain tumor imaging including L-[^{11}C]methionine ([^{18}F]MET), *O*-(2-[^{18}F]fluoroethyl)-L-tyrosine ([^{18}F]FET) and 6-[^{18}F]fluoro-3,4-dihydroxy-L-phenylalanine ([^{18}F]FDOPA).[4-12] Certain radiolabeled amino acids have also shown promising imaging properties for other types of tumors such as neuroendocrine tumors with [^{18}F]FDOPA and prostate cancer with *anti*-1-amino-3-[^{18}F]fluorocyclobutyl-1-carboxylic acid (*anti*-3-[^{18}F]FACBC).[13-17]

A range of amino acid transporter systems and substrates have been shown to be relevant to oncologic imaging, and there has been recent interest in PET tracers targeting glutamine transport and metabolism. The metabolically inert tracer *anti*-3-[^{18}F]FACBC has been shown to be a substrate for ASCT2, an important glutamine transporter in cancer, and to a lesser extent system L and system A, in human prostate cancer cells.[18, 19] Human studies indicate that *anti*-3-[^{18}F]FACBC has clinical potential for imaging prostate cancer and brain tumors.[20, 21] Another strategy for targeting glutamine metabolism in cancer has employed a series of ^{18}F-labeled analogues of glutamine. In particular, 4-[^{18}F]-(2*S*,4*R*)-fluoroglutamine ([^{18}F]-FGln) has been shown to be promising in human studies for monitoring progression of gliomas.[22-24]Additionally, the ^{18}F-tracer targeting system ASC, 3-(1-[^{18}F]fluoromethyl)-L-alanine (L-[^{18}F]FMA) was shown to be a potential useful PET tracer in preclinical studies.[25] A limitation of the tracers FGln and FMA has been in vivo defluorination. There has also been recent interest in glutamate analogues and other amino acids bearing carboxylic acids on their side chains targeting system x_C^- which is upregulated in many cancers and a marker of tumor oxidative stress.[26-28] Finally, lead compounds targeting cationic amino acid transporters including (*S*)-2-amino-3-[1-(2-[^{18}F]fluoroethyl)-1H-

[1,2,3]triazol-4-yl]propanoic acid ((*S*)-[^{18}F]AFETP) and *N*-2-[^{18}F]fluoroethyl-*N*-methyl-2-aminoethyl-tyrosine ([^{18}F]FEMAET) have been recently developed and reported.[2, 29, 30]

An important limitation of system L transport substrates as imaging agents is the inability of system L transporters to directly concentrate substrates intracellularly. This property leads to relative low tumor to tissue ratios which can reduce sensitivity for lesion detection and lead to washout of activity from tumors over time. Other amino acid transporters including system A transporters can concentrate substrates intracellularly, providing higher and more persistent uptake in tumors. However, the lack of activity of many amino acid transporters at the luminal side of the BBB limits access of their substrates to the enhancing regions of brain tumors. These observations prompted us to develop ^{18}F-labeled amino acid tracers that target both system L and non-system L amino acid transporters in an effort to maintain brain availability through system L transport while enhancing tumor to normal tissue ratios through non-system L transporters. In our previously reports of the synthesis and biological evaluation of three α,α-disubstituted amino acids with varying selectivities for system A and system L transporters: 3-[^{18}F]fluoro-2-methyl-2-*N*-(methylamino)propanoic acid ([^{18}F]MeFAMP), 2-amino-3-[^{18}F]fluoro-2-methylpropanoic acid ([^{18}F]FAMP), and 2-amino-4-[^{18}F]fluoro-2-methylbutanoic acid ([^{18}F]FAMB),[31-33] we proposed to develop new ^{18}F-labeled analogues with longer alkyl chain lengths to increase recognition by system L transporters and thereby improve brain availability.

Here, we report efficient organic and radiosynthetic routes to obtain the (*R*)- and the (*S*)-enantiomers of 2-amino-5-[^{18}F]fluoro-2-methylpentanoic acid ([^{18}F]FAMPe), an analogue of [^{18}F]FAMP and [^{18}F]FAMB. These novel tracers were evaluated in the mouse DBT (delayed brain tumor) model of glioblastoma through in vitro uptake assays, biodistribution studies, and small animal PET/CT imaging.[2, 34] The tumor and the brain uptake of (*R*)- and (*S*)-[^{18}F]**8** ((*R*)- and (*S*)-[^{18}F]FAMPe) were compared with the established system L PET tracer, (*S*)-[^{18}F]FET, and the system A PET tracer (*R*)-[^{18}F]MeFAMP through small animal PET studies. (*S*)-[^{18}F]**8** demonstrated very high uptake in this tumor model and

increased recognition by system L transport compared to (*R*)-[^{18}F]MeFAMP. However, the longer side chain led to loss of recognition by system A transporters with recognition by other neutral amino acid transporters including glutamine transport systems.

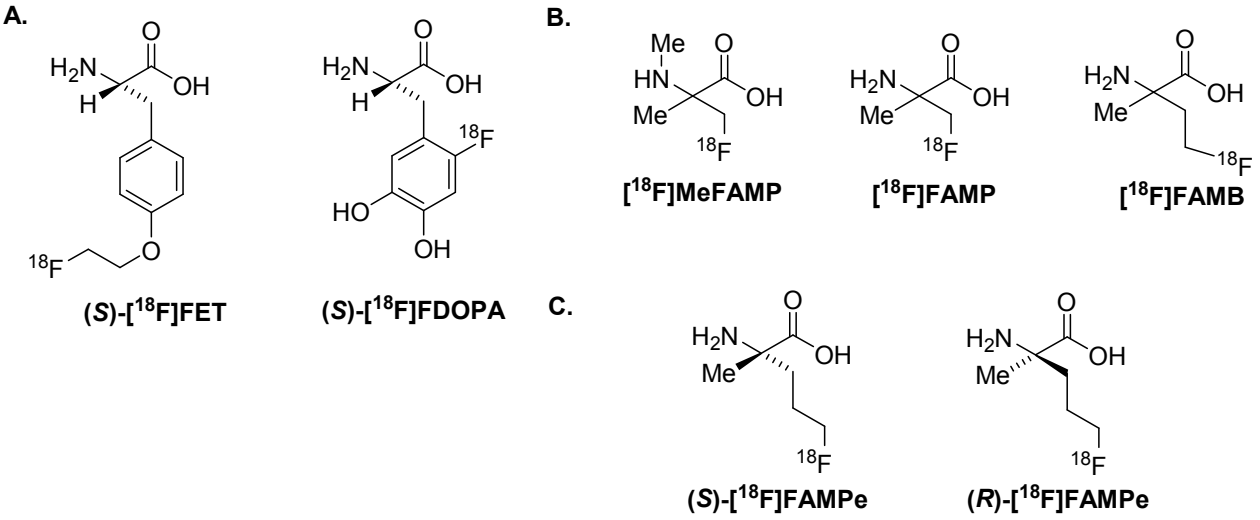

Figure 1: Selected ^{18}F-labeled amino acids. (**A**) Both [^{18}F]FET and [^{18}F]FDPOA have been used for imaging brain tumors in human subjects. (**B**) [^{18}F]FAMP, [^{18}F]FAMB, and [^{18}F]MeFAMP are α,α-disubstituted amino acids; (*R*)-[^{18}F]MeFAMP is an established substrate for system A transport. (**C**) (*S*)- and (*R*)-[^{18}F]FAMPe are novel α,α-disubstituted amino acids evaluated in this publication in the DBT glioma model.

Results and Discussion

1. Chemistry.

The racemic non-radioactive forms of the amino acid 2-amino-5-fluoro-2-methylpentanoic acid ((*R,S*)-**8**) were prepared in a simple eight step synthesis as shown in **Scheme 1**. From commercially available L-alanine *tert*-butyl ester hydrochloride and benzophenone imine, we synthesized in very good yield (94%) and without further purification our first intermediate which is the ester imine derivative of alanine, *tert*-butyl 2-((diphenylmethylene)amino)propanoate ((*S*)-**1**). In a second step, we conducted a non-stereoselective alkylation with allyl iodide at the α-carbon of the amino acid derivative which

provided *tert*-butyl (*R,S*)-2-((diphenylmethylene)amino)-2-methylpent-4-enoate ((*R,S*)-**2**), also in very good yield (90%). After the simple and rapid hydrolysis of the imine function of (*R,S*)-**2** with hydroxylamine hydrochloride at room temperature, we obtained the amino acid ester *tert*-butyl (*R,S*)-2-amino-2-methylpent-4-enoate ((*R,S*)-**3**). The following step protected this amine in presence of di-*tert*-butyl dicarbonate which gave *tert*-butyl (*R,S*)-2-((tert-butoxycarbonyl)amino)-2-methylpent-4-enoate ((*R,S*)-**4**) in very good yield (92%). Then, an hydroboration of the alkene followed by hydrolysis in presence of 30% hydrogen peroxide provided the desired terminal alcohol intermediate, *tert*-butyl (*R,S*)-2-((*tert*-butoxycarbonyl)amino)-5-hydroxy-2-methylpentanoate ((*R,S*)-**5**) in a good yield (62%). The alcohol was converted into a leaving group through tosylation to provide the racemic labeling precursor *tert*-butyl (*R,S*)-2-((tert-butoxycarbonyl)amino)-2-methyl-5-(tosyloxy)pentanoate ((*R,S*)-**6**) in moderate yield (40%).

To perform the nucleophilic substitution of the tosylate group with non-radioactive fluoride, we tried several different conditions. Our first attempt consisted of treating the tosylate compound (*R,S*)-**6** with an excess of tetrabutylammonium fluoride in acetonitrile at room temperature. The reaction consumed the starting material to provide a single major product in 86%, but instead of the desired product, an intramolecular cyclization occurred to form di-*tert*-butyl (*R,S*)-2-methylpyrrolidine-1,2-dicarboxylate ((*R,S*)-**9**) as shown in **Scheme 2**. This reaction gave only trace quantities of the desired fluoro product *tert*-butyl (*R,S*)-2-((tert-butoxycarbonyl)amino)-5-fluoro-2-methylpentanoate ((*R,S*)-**7**). Because a similar reaction proceeded without this difficulty in the synthesis of FAMB (one carbon shorter side chain),[32] the favorable kinetics of the intramolecular formation of a five ring cycle is the likely cause in this case. Attempts to form the di-Boc protected nitrogen compound as has been reported in the synthesis of fluoroleucine derivatives were not successful.[35] We thus followed a different protocol in which the authors used *tert*-amyl alcohol (2-methylbutan-2-ol) as solvent for nucleophilic fluorination reactions.[36] The authors suggested that the *tert*-amyl alcohol solvent system might have four beneficial influences on the mechanism of this fluorination process: (*i*) the hydrogen bond between the *tert*-amyl

alcohol solvent and the fluoride may reduce the strength of the CsF ionic bond, (*ii*) the solvation of fluoride will be limited and thus fluoride will be a good nucleophile due to the bulky *tert*-amyl alcohol, (*iii*) the hydrogen bond between the *tert*-amyl alcohol solvent and the oxygen atoms of a sulfonate leaving group may enhance the leaving group reactivity, and (*iv*) the protic environment of the reaction medium, as well as hydrogen bonding between the *tert*-amyl alcohol and reactive heteroatoms in the substrate, may reduce side reactions such as intramolecular cyclization. By using three equivalents of cesium fluoride (CsF) in *tert*-amyl alcohol (2-methylbutan-2-ol) at 80 °C, we obtained the desired fluoro compound (*R,S*)-**7** and also the cyclic compound (*R,S*)-**9** after 1 h, but approximately 15% of starting material (*R,S*)-**6** remained. By increasing the amount of CsF used to five equivalents and the temperature to 100 °C without reaching reflux, the reaction was completed in 1 h, and the fluoro compound (*R,S*)-**7** was obtained in 34% yield. We also conducted the reaction in the presence of ten equivalents of CsF but the same yield was obtained. Thus, Kim's methodology allowed us to obtain the desired product (*R,S*)-**7** in acceptable yields. The final step consisted of the deprotection of (*R,S*)-**7**. The deprotection was achieved with 4 M hydrochloric acid at 60 °C which provided the racemic non-radioactive amino acid (*R,S*)-**8** as the hydrochloride salt in good yield (78%) and high purity.

Scheme 1: Multistep synthesis of the racemic non-radioactive amino acid (*R,S*)-**8**.

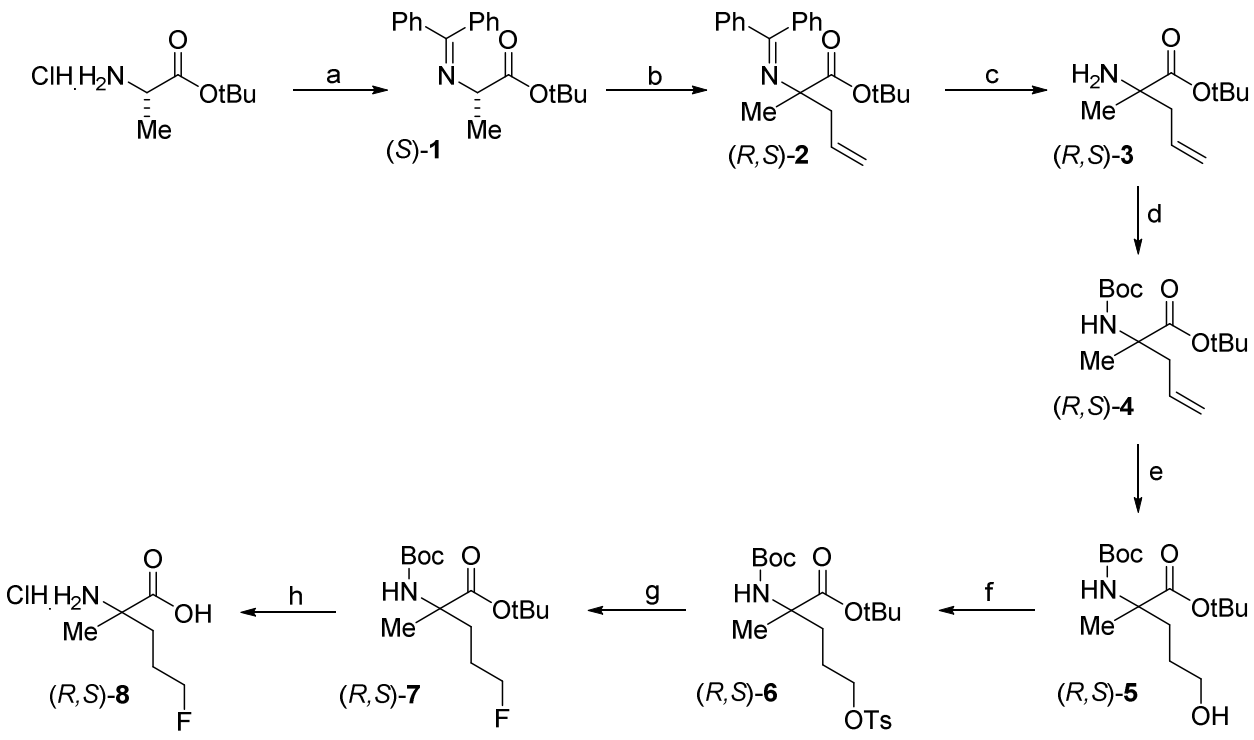

Reagents and conditions: a) diphenylmethanimine, DCM, rt, 2 h; b) LDA, 3-iodoprop-1-ene, THF, -78 °C then rt for 18 h; c) NH_2OH, MeOH, rt, 1 h; d) Boc_2O, THF, rt, 18 h; e) BH_3.THF then NaOH 1 M, H_2O_2 30%, 0 °C then rt for 18 h; f) TsCl, NaOtBu, DCM, 0 °C then rt for 18 h; g) CsF, 2-methylbutan-2-ol, 100 °C, 1h; h) HCl 4 M, 60 °C, 90 min.

Scheme 2: Reaction conditions (equivalents of fluoride, solvent and temperature) were optimized to minimize the cyclized compound (*R*,*S*)-**9**.

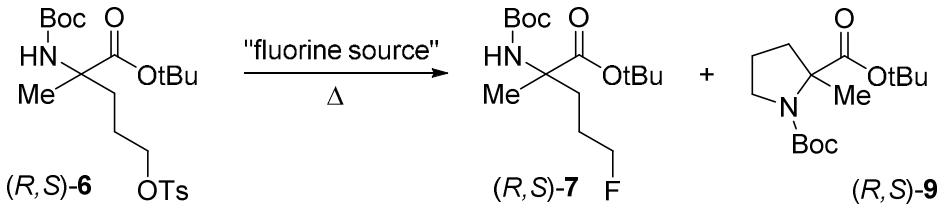

To obtain the enantiomerically pure radiolabeling precursors, tosylate precursors (*S*)-**6** and (*R*)-**6** were prepared in four steps started with the commercially available starting materials (*S*)-(-)-α-allylalanine and

(*R*)-(+)-α-allylalanine respectively (see **Scheme 3**). During the first step, (*S*)-α-allylalanine and (*R*)-α-allylalanine were treated with di-*tert*-butyl dicarbonate to give the carbamates *(R)- and (S)*-2-((*tert*-butoxycarbonyl)amino)-2-methylpent-4-enoic acid ((*S*)-**10** and (*R*)-**10**), respectively, which were used without purification in the next reaction. The second step consisted of the protection of the carboxylic acid function of (*S*)-**10** and (*R*)-**10** by using *N,N*-dimethylformamide *di*-tert-butyl acetal; compounds (*S*)-**4** and (*R*)-**4** were thus obtained. Then, as previously described for the racemic mixture (*R,S*)-**4**, the alkene on the alkyl chain was converted into a terminal alcohol which provided products (*S*)-**5** and (*R*)-**5**. In the last step, these compounds were converted into tosylates to provide the radiolabeling precursors (*S*)-**6** and (*R*)-**6**. Each enantiomerically pure radiolabeling precursor was obtained in similarly good yield.

Scheme 3: Synthesis of the tosylate precursors (*S*)-**6** and (*R*)-**6** for radiolabeling.

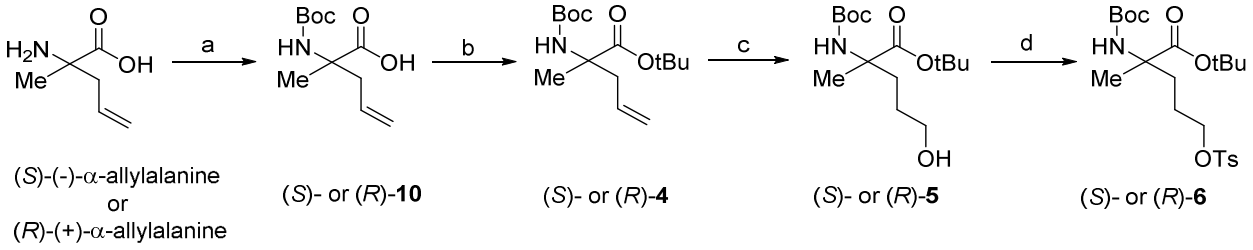

Reagents and conditions: a) Boc_2O, MeOH/NEt_3/NaOH 1 M for 18 h; b) *N,N*-dimethylformamide di-*tert*-butyl acetal, anhyd toluene for 2 h at 90 °C then 18 h at rt; c) BH_3.THF then NaOH 1 M, H_2O_2 30%, 0 °C then rt for 18 h; f) TsCl, NaOtBu, DCM, 0 °C then rt for 18 h.

2. Radiochemistry.

The radiosynthesis was conducted in two steps (see **Scheme 4**). The first step, nucleophilic [^{18}F]fluoride substitution, was successfully performed in *tert*-amyl alcohol (2-methylbutan-2-ol) at 96-105 °C to afford the intermediates (*S*)-[^{18}F]**7** and (*R*)-[^{18}F]**7** from the appropriate enantiomerically pure precursor. Using solid phase extraction with a C_{18} cartridge, the ^{18}F-labeled intermediate was retained while the unreacted

[^{18}F]fluoride was removed. Then, the ^{18}F-labeled intermediate was eluted from the cartridge with acetonitrile and purified by reverse-phase high performance liquid chromatography (HPLC). The collected fractions from HPLC containing the ^{18}F-labeled intermediate were combined, diluted with water, and passed through a light hydrophilic-lipophilic-balanced (HLB) cartridge which was rinsed two more times with water in order to remove residual acetonitrile. The intermediates, (*S*)-[^{18}F]**7** or (*R*)-[^{18}F]**7**, were then eluted with a small amount of ethanol. In a second step, a quantitative deprotection was achieved with aqueous hydrochloric acid and followed by elution through a cartridge allowing the neutralization of highly acidic sample to provide the final product (*S*)-[^{18}F]**8** or (*R*)-[^{18}F]**8** which were obtained in 24% to 52% (n= 8) decay corrected yields respectively, at pH= 6 and over 99% radiochemical purity determined by radiometric thin-layer chromatography and analytic HPLC (see **Figure 2**). In a representative synthesis, a total of 9.9 mCi of (*R*)-[^{18}F]**8** at end of synthesis (EOS) was obtained from 40.8 mCi of [^{18}F]fluoride after the drying process in a synthesis time of approximately 120 min using 5 mg of the tosylate precursor (*R*)-**6**. The specific activity was > 1 Ci/μmol at the end of synthesis. Sterile water was used for formulation of the final product for cell uptake assays to avoid the presence of sodium ions in the sodium-free uptake conditions. For the animal studies, the solution was passed through a 0.22 μm nylon filter, and then adjusted to a concentration of 0.9% sodium chloride. The stability of (*S*)-[^{18}F]**8** and (*R*)-[^{18}F]**8** up to 6 h after formulation was confirmed by analytical HPLC.

Scheme 4: Radiosynthesis of (*S*)-[^{18}F]**8**.

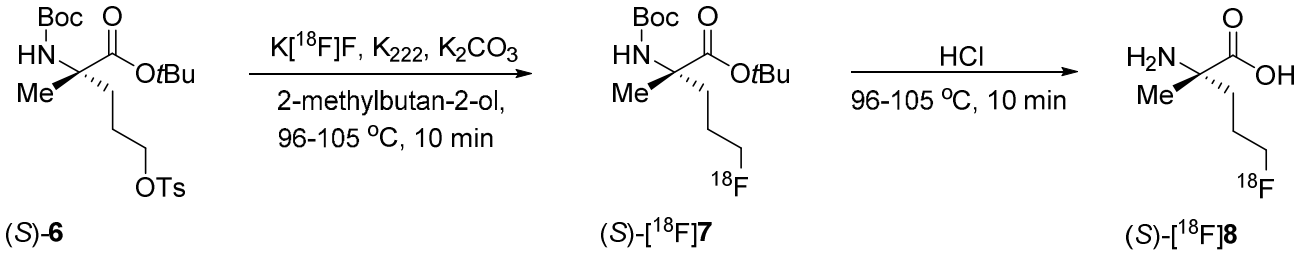

(*S*)-**6** (*S*)-[^{18}F]**7** (*S*)-[^{18}F]**8**

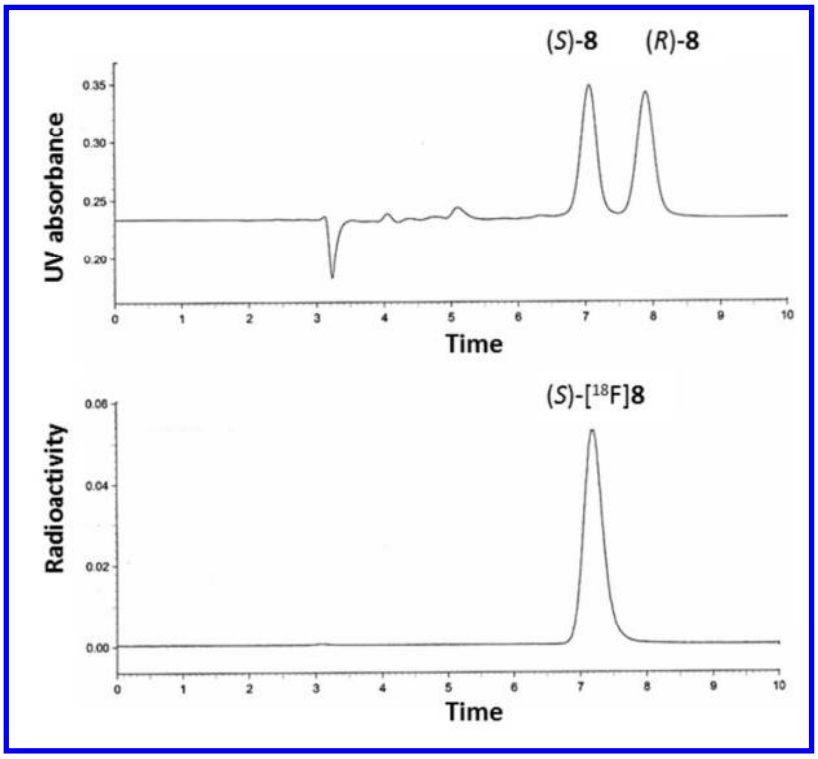

Figure 2: Analytical chiral HPLC co-injections of a mixture of the non-radioactive racemic product (*R,S*)**-8** (seen with UV detection) and (*S*)-[^{18}F]**8** (seen with radiometric detection).

3. Cell uptake assays.

Amino acid uptake assays were performed using mouse DBT glioma cells in the presence and absence of two well-described inhibitors of amino acid transport, *N*-methyl α-aminoisobutyric acid (MeAIB) and 2-amino-bicyclo[2.2.1]-heptane-2-carboxylic acid (BCH), which were used as inhibitors for system A and system L, respectively. These two commonly used inhibitors allowed us to evaluate the contribution of these amino acid transport systems to the cellular uptake of (*S*)- and (*R*)-[^{18}F]**8**. The results of the in vitro cell uptake assays are shown in **Figure 3**. The two enantiomers were compared to (*R*)-[^{18}F]MeFAMP, a good substrate for system A amino transport, and (*S*)-[^{18}F]FET, a well-characterized system L transport substrate. The uptake assays were performed with a brief (30 or 60 seconds) uptake time to evaluate the initial influx of (*S*)- or (*R*)-[^{18}F]**8** and minimize the potential for efflux which occurs with many amino acid transporters including system L and ASC. An additional set of inhibition

experiments shown in **Figure 4** were performed using varying concentrations of L-glutamine (Gln) to establish the role of glutamine transporters in the uptake of (*S*)- and (*R*)-[^{18}F]**8**.

Certain amino acids transporters including system A and system ASC require co-transport of sodium ions to function while others including system L function in sodium-free conditions. Thus, we compared uptake in the presence of sodium ions and under sodium-free conditions using the cation choline as a substitute for sodium ions. In presence of MeAIB, there was no significant inhibition uptake of (*S*)-[^{18}F]**8**, indicating that system A transport does not play a substantial role in the in vitro uptake of this tracers by DBT cells. A minor component of inhibition of (*R*)-[^{18}F]**8** was observed with MeAIB (83 ± 17% uptake relative to control, $p < 0.05$). These results are similar to the ones obtained with the structurally similar compound, [^{18}F]FMA, developed by Wang *et al*., as uptake of this tracer by 9L glioma cells was not inhibited by MeAIB.[25] Substitution of choline for sodium ions resulted in partial inhibition of uptake of both enantiomers with 71 ± 17 % uptake relative to control for (*S*)-[^{18}F]**8** and 70 ± 11% for (*R*)-[^{18}F]**8**. These results indicate that both enantiomers enter DBT cells partly via sodium-dependent amino acid transport, but not via the sodium-dependent system A, as shown by the lack of uptake inhibition by MeAIB. In the presence of MeAIB, the uptake of the system A substrate (*R*)-[^{18}F]MeFAMP was 19 ± 9% relative to the sodium control which is consistent with prior reports that (*R*)-[^{18}F]MeFAMP is a good substrate for system A in a range of rodent and human cancer cell lines.[31, 33, 37] Similarly, the uptake of (*R*)-[^{18}F]MeFAMP was reduced to 21 ± 19% relative to the sodium control in the sodium-free choline condition, consistent with sodium-dependence of system A transport and demonstrating that (*R*)-[^{18}F]MeFAMP enter DBT cells mainly via the system A amino acid transport. As expected, uptake of the system L transport substrate (*S*)-[^{18}F]FET by DBT cells was not significantly inhibited by MeAIB, inhibitor of the system A amino acid transporter, or by sodium-free conditions as system L is sodium-independent.

BCH is commonly used as a competitive antagonist of the sodium-independent L type transport system, but also competitively inhibits amino acid uptake via the sodium-dependent $B^{0,+}$ and B^0 transport system. In the presence of sodium, BCH reduced the uptake of (*S*)-[^{18}F]**8** to 59 ± 15% relative to control

and reduced the uptake of (*R*)-[^{18}F]**8** to 47 ± 12% relative to control. In the absence of sodium, the addition of BCH reduced the uptake of (*S*)-[^{18}F]**8** and (*R*)-[^{18}F]**8** to 72 ± 11% ($p = 0.017$) and 46 ± 4% ($p < 0.001$) respectively, relative to the choline control condition. These results indicate a component of system L transport of both compounds. In the case of (*R*)-[^{18}F]MeFAMP, no significant inhibition was observed in the presence of sodium BCH relative to control. In contrast, almost all of the uptake of (*S*)-[^{18}F]FET was inhibited by BCH in the presence and absence of sodium ($p < 0.01$), consistent with prior studies showing (*S*)-[^{18}F]FET is substrate for system L amino acid transport.[9]

Equal concentrations of the amino acids alanine, serine, and cysteine (ASC) were also used for uptake inhibition as these amino acids are competitive inhibitors for many neutral amino acid transporters including system A, system ASC, and to a lesser extent system L. In the sodium ASC condition, the uptake of (*S*)-[^{18}F]**8** and (*R*)-[^{18}F]**8** were reduced to 52 ± 14% and 41 ± 4%, respectively, relative to the sodium control ($p < 0.001$ for both). These results indicate that (*R*)- and (*S*)-[^{18}F]**8** undergo uptake by non-system A neutral amino acid transport in addition to a component of system L transport. In the case of (*R*)-[^{18}F]MeFAMP, the ASC condition reduced the uptake of (*R*)-[^{18}F]MeFAMP to 22 ± 9% relative to the sodium control ($p < 0.001$); the uptake of (*S*)-[^{18}F]FET was reduced by approximately 40% but did not reach statistical significance.

Because glutamine is an important amino acid in cancer metabolism and the ASC condition is expected to inhibit glutamine uptake, additional uptake assays were performed in presence of different concentrations of glutamine (0.1, 1.0 and 10 mM) and ASC (1 mM and 10 mM) as shown in **Figure 4**. The results demonstrated that (*S*)-[^{18}F]**8** uptake was more sensitive to glutamine and ASC inhibition than (*R*)-[^{18}F]**8**. The uptake of (*S*)-[^{18}F]**8** was blocked in a dose-dependent manner by glutamine and ASC; in contrast, significant inhibition of (*R*)-[^{18}F]**8** did not occur in the presence of glutamine and was observed only with the 10 mM ASC condition. At the 1 mM and 10 mM concentration of glutamine, the uptake of (*S*)-[^{18}F]**8** was respectively reduced to 76 ± 21% ($p < 0.05$) and 66 ± 9% ($p < 0.001$) relative to the control value. Similarly, at the 1 mM and 10 mM concentrations of ASC, the uptake of (*S*)-[^{18}F]**8** uptake was respectively reduced to 61 ± 16% ($p < 0.01$) and 38 ± 9% relative to the control value. In contrast, only

the 10 mM concentration of ASC caused a significant reduction of (*R*)-[^{18}F]**8** uptake (49 ± 9% relative to control, $p < 0.001$). These data suggest that (*S*)-[^{18}F]**8** uptake by DBT cells is partly mediated by amino acid transporters that recognize glutamine.

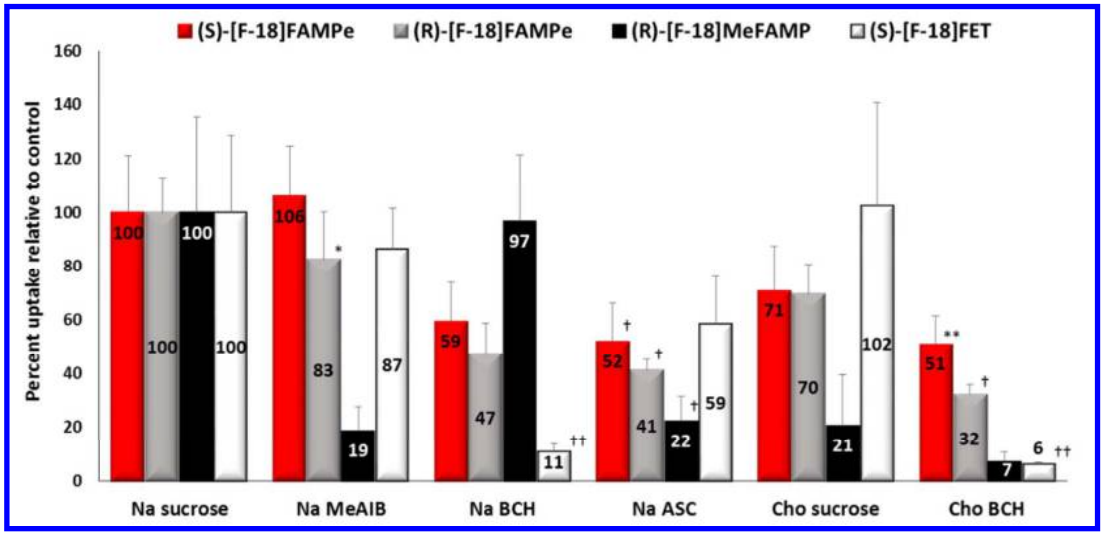

Figure 3: In vitro uptake of (*S*)- and (*R*)-[^{18}F]**8**, (*R*)-[^{18}F]MeFAMP and (*S*)-[^{18}F]FET in DBT glioma cells in presence and absence of competitive inhibitors of amino acid transport. The uptake data are normalized based on the amount of activity added to each well and the total amount of protein in each well. The data are expressed as percentage uptake relative to the sodium control condition, and the values for each condition are noted in the appropriate bars. The number of replicates per condition were 7 or 8 for (*S*)- and (*R*)-[^{18}F]**8** and 3 or 4 for (*R*)-[^{18}F]MeFAMP and (*S*)-[^{18}F]FET. Na control and Cho control contain 10 mM sucrose to provide an osmolarity consistent with the inhibitory conditions. Na= assay buffer containing sodium ions; Cho= assay buffer containing choline ions; MeAIB= 10 mM *N*-methyl α-aminoisobutyric acid (system A inhibitor); BCH= 10 mM 2-amino-bicyclo[2.2.1]-heptane-2-carboxylic acid (system L inhibitor); ASC= 3.3 mM each of L-Ala, L-Ser, L-Cys. *p*-values represent comparisons of uptake in the presence of inhibitor to control uptake for each radiotracer (1-way ANOVA) with Dunnett's multiple comparison post-tests . The choline sucrose control condition was compared to the choline BCH condition using a 2-sided t-tests. * = $p < 0.05$, ** = $p = 0.017$, † = $p < 0.001$, and †† = $p < 0.01$.

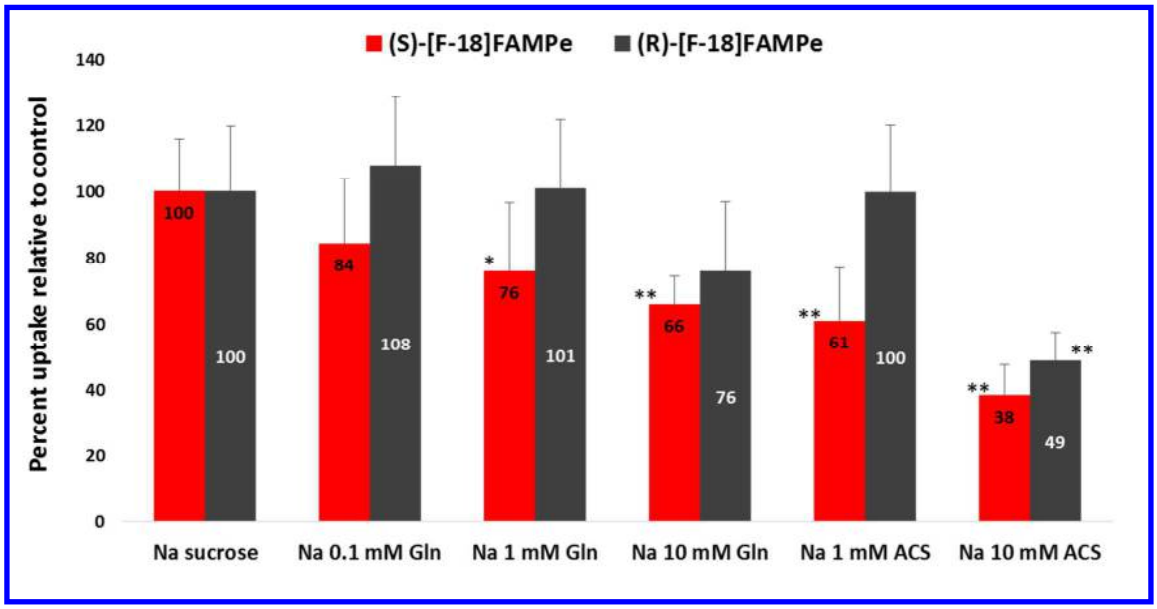

Figure 4: In vitro uptake of the two enantiomers (*S*)- and (*R*)-[^{18}F]**8** in DBT glioma cells in presence and absence of competitive inhibitors of amino acid transport. The uptake data are normalized based on the amount of activity added to each well and the total amount of protein in each well. The data are expressed as percentage uptake relative to the sodium control condition, and the values for each condition are noted in the appropriate bars. Replicates per condition (n= 8). To provide a consistent osmolarity compared to the inhibitory conditions, Na control contain 10 mM sucrose. Na= assay buffer containing sodium ions; Gln= glutamine; 10 mM ASC= 3.3 mM each of L-Ala, L-Ser, L-Cys. *p*-Values represent comparisons of uptake in the presence of inhibitor to control uptake for each radiotracer (1-way ANOVA) with Dunnett's multiple comparison post-tests. * = $p < 0.05$, ** = $p < 0.001$.

Taken together, these in vitro inhibition studies indicate that (*S*)-[^{18}F]**8** and (*R*)-[^{18}F]**8** entered DBT cells predominantly via sodium-independent amino acid transporters including a component of system L transport. Additionally, (*S*)-[^{18}F]**8** uptake appears to be mediated in part by amino acid transporters that recognize glutamine, although defining the specific transporter systems involved will require further characterization. Because of the importance of glutamine in cancer metabolism, (*S*)-[^{18}F]**8** may serve as a lead compound for developing more selective probes for glutamine transport. There is a growing evidence that certain system L and system ASC amino acid transporters, in particular LAT1 and ASCT2, are involved in signaling including the mTOR pathways, promote tumor growth, and have prognostic significance.[1, 4, 38-43]

4. Biodistribution studies in mice with subcutaneous DBT glioma

The results of biodistribution studies with each enantiomer of [^{18}F]**8** in BALB/c mice with subcutaneous DBT tumors 5, 30, and 60 min post-injection (p.i.) are shown in **Table 1** and expressed as percent of total injected dose per gram of tissue (%ID/g). The results demonstrated good tumor uptake of radioactivity at the different time points p.i. for both (*S*)- and (*R*)-[^{18}F]**8** with progressive increase over time for the (*S*)-enantiomer. The uptake in the brain also increases for both enantiomers but to a lesser extent than the tumor. At each time point, the uptake of both (*S*)- and (*R*)-[^{18}F]**8** in subcutaneous glioma was higher than normal brain ($p < 0.001$).

The tumor uptake of activity of (*S*)-[^{18}F]**8** after injection was very rapid with 5.1 ± 0.45 %ID/g at 5 min, and increased to 7.4 ± 0.87 %ID/g at 30 min and 9.9 ± 2.5 %ID/g at 60 min. For (*R*)-[^{18}F]**8**, similar tumor uptake was observed at 5 min with a value of 3.7 ± 0.60 %ID/g. The uptake of (*R*)-[^{18}F]**8** did not increase to the same extent over time as with (*S*)-[^{18}F]**8**, and (*R*)-[^{18}F]**8** led to 4.2 ± 0.49 %ID/g at 30 min and 3.3 ± 0.65 %ID/g at 60 min. The tumor uptake of (*R*)-[^{18}F]**8** decreased slightly between 30 and 60 min while uptake of (*S*)-[^{18}F]**8** increased between these time points. The tumor uptake of (*S*)-[^{18}F]**8** was significantly higher than with (*R*)-[^{18}F]**8** at 30 and 60 min after injection ($p < 0.01$ and $p < 0.001$, respectively). Moreover, 1 h after injection the value of the uptake of (*S*)-[^{18}F]**8** was three time that of (*R*)-[^{18}F]**8**. Similarly, the normal brain uptake was significantly higher with (*S*)-[^{18}F]**8** than with (*R*)-[^{18}F]**8** with 0.65 ± 0.06 %ID/g 5 min after injection versus 0.48 ± 0.07 %ID/g, respectively ($p < 0.05$). The uptake increased very little at 30 min post injection for both enantiomers, but increased more at 60 min p.i with 0.85 ± 0.08 %ID/g for (*S*)-[^{18}F]**8** compared to 0.56 ± 0.13 %ID/g for (*R*)-[^{18}F]**8** ($p < 0.001$). The biodistribution studies showed a higher activity in the blood for (*S*)-[^{18}F]**8** than for (*R*)-[^{18}F]**8** with 8.9 ± 0.3 %ID/g and 5.7 ± 0.7 %ID/g respectively at 5 min p.i. with slower clearance of (*S*)-[^{18}F]**8** than for (*R*)-[^{18}F]**8** at the 60 min time point.

As shown in **Figure 5**, tumor to brain ratios for (*S*)-[^{18}F]**8** ranged from 7.9 to 11.8 and increased over the course of the study. Tumor to brain ratios for (*R*)-[^{18}F]**8** started at 7.7, increased to 8.6 at 30 min p.i., and finally decreased to 5.8 at 1 h. The tumor to brain ratios were higher for (*S*)-[^{18}F]**8** than for the *R*-

enantiomer, primarily due to the higher tumor uptake of (*S*)-[^{18}F]**8**. Differential transport and biological properties of enantiomers of radiolabeled amino acids has been described in the literature for many radiolabeled compounds. For example, the system A substrate (*R*)-[^{18}F]MeFAMP showed higher tumor uptake than (*S*)-[^{18}F]MeFAMP in a range of human tumor xenograft models.[31] Our results demonstrate the importance of assessment of the in vitro and in vivo biological properties for both enantiomers, as (*S*)-[^{18}F]**8** appeared to be the more promising enantiomer for imaging due to substantially higher uptake in tumors and normal brain.

Table 1: Biodistribution of (*S*)- and (*R*)-[^{18}F]**8** in BALB/c mice with subcutaneous DBT tumors.

	5min		30min		60min	
	(*S*)-[F-18]FAMPe	(*R*)-[F-18]FAMPe	(*S*)-[F-18]FAMPe	(*R*)-[F-18]FAMPe	(*S*)-[F-18]FAMPe	(*R*)-[F-18]FAMPe
blood	8.86 +/- 0.31	5.67 +/- 0.75	*4.82* +/- 0.38	*1.79* +/- 0.24	3.88 +/- 0.42	1.05 +/- 0.22
bone	2.69 +/- 0.17	2.25 +/- 0.73	3.96 +/- 0.29	2.55 +/- 0.90	6.33 +/- 0.96	2.91 +/- 0.86
brain	*0.65 +/- 0.06* †	*0.48 +/- 0.07* †	*0.68 +/- 0.06* ††	*0.49 +/- 0.05* ††	*0.85 +/- 0.08* *†	*0.56 +/- 0.13* *†
fat	1.42 +/- 0.19	1.77 +/- 0.62	0.91 +/- 0.15	1.15 +/- 0.54	0.77 +/- 0.15	0.41 +/- 0.13
heart	3.24 +/- 0.49	2.21 +/- 0.43	2.91 +/- 0.22	1.50 +/- 0.36	2.89 +/- 0.29	1.16 +/- 0.19
kidney	14.89 +/- 2.89	18.90 +/- 2.21	15.40 +/- 1.31	8.04 +/- 1.60	13.02 +/- 4.26	4.72 +/- 1.06
liver	4.30 +/- 0.38	2.74 +/- 0.29	4.67 +/- 0.43	2.31 +/- 0.26	4.30 +/- 0.41	1.46 +/- 0.39
lung	9.10 +/- 0.63	7.37 +/- 0.83	4.91 +/- 0.53	2.85 +/- 0.40	4.05 +/- 0.45	1.65 +/- 0.40
muscle	2.10 +/- 0.13	1.52 +/- 0.28	1.95 +/- 0.19	1.15 +/- 0.29	2.14 +/- 0.24	1.00 +/- 0.17
pancreas	34.09 +/- 5.07	25.68 +/- 4.21	53.06 +/- 14.34	21.16 +/- 6.22	47.33 +/- 15.72	11.62 +/- 3.90
spleen	5.77 +/- 0.37	4.28 +/- 0.76	5.82 +/- 0.77	2.51 +/- 0.41	5.05 +/- 0.49	1.96 +/- 0.42
thyroid	3.82 +/- 0.89	3.13 +/- 0.81	3.56 +/- 0.45	1.74 +/- 0.30	3.86 +/- 0.18	1.39 +/- 0.40
tumor	5.09 +/- 0.45	3.68 +/- 0.60	*7.37 +/- 0.87* *	*4.20 +/- 0.49* *	*9.88 +/- 2.48* **	*3.27 +/- 0.65* **

Mice were not anesthetized for the biodistribution studies. 23 μCi (0.85 MBq) of (*S*)-[^{18}F]**8**, and 29 μCi (1.07 MBq) of (*R*)-[^{18}F]**8** were administrated via tail vein injection. The animals were euthanized after 5, 30, and 60 min in group of 5 animals. The data are expressed as %ID/g and errors are expressed as standard deviation. *p*-Values represent comparisons of uptake data for (*S*)- versus (*R*)-[^{18}F]**8** in tumor and brain tissue through 1-way ANOVA with Tukey post-tests. * = $p < 0.01$, **, ††,*† = $p < 0.001$, † = $p < 0.05$.

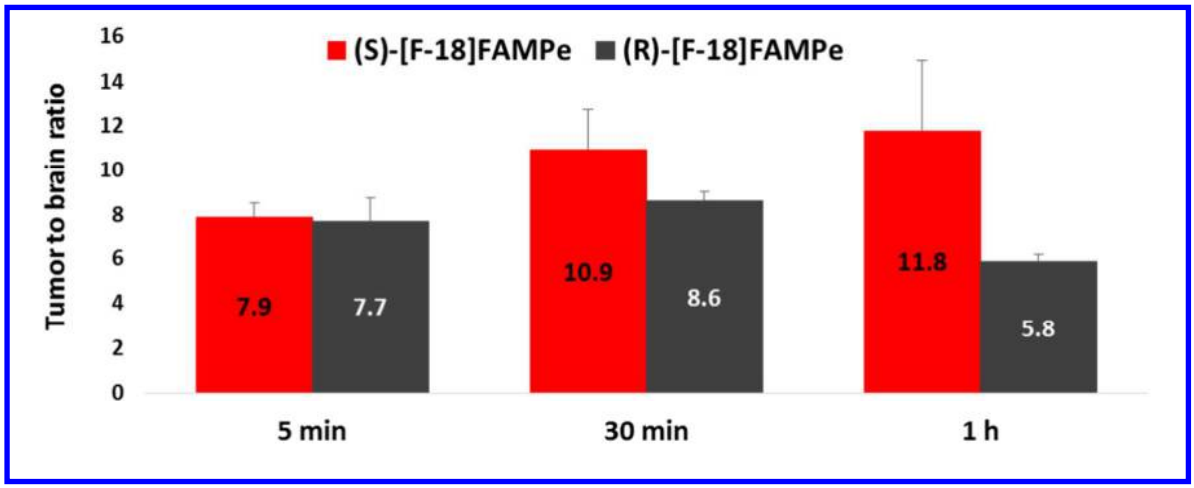

Figure 5: Tumor to brain ratios from biodistribution studies conducted in BALB/c mice with subcutaneous DBT tumors.

As for the brain and DBT tumor, (*S*)-[^{18}F]**8** demonstrated higher uptake than (*R*)-[^{18}F]**8** in most of the normal organs at all time points evaluated. The highest levels of uptake for (*S*)- and (*R*)-[^{18}F]**8** at all time points were observed in the kidneys and pancreas, a pattern frequently seen with radiolabeled amino acids. Although excretion in the urine and feces was not measured, the high kidney uptake and bladder activity observed in the small animal PET studies suggests a renal route of excretion for these tracers. For other organs including the heart, liver, and muscle the uptake was low to moderate for both enantiomers (from 1 to 4.67 %ID/g during the study) with about two-fold more uptake for (*S*)-[^{18}F]**8** than (*R*)-[^{18}F]**8** in most tissues. Bone activity was low and constant for (*R*)-[^{18}F]**8** (from 2.25 ± 0.73 %ID/g to 2.91 ± 0.86 %ID/g) while it was little higher and slowly increased over time for (*S*)-[^{18}F]**8** (from 2.69 ± 0.17 %ID/g to 6.33 ± 0.96 %ID/g). The increasing bone activity observed with (*S*)-[^{18}F]**8** may result from in vivo defluorination but could potentially represent accumulation in the bone marrow. The tumor to bone ratio for (*S*)-[^{18}F]**8** at 60 min after injection was approximately 1.5 which is much higher than the ratio observed with the structurally related compound [^{18}F]FMA,[25] consistent with less in vivo defluorination due to the presence of the α-methyl group in (*S*)-[^{18}F]**8.**

5. Small animal PET/CT studies in mice with intracranial DBT tumors

The results from small animal PET studies in mice with intracranial DBT tumors are presented as time activity curves (TACs) in **Figure 6**. The results showing average standardized uptake values (SUVs) obtained with (*S*)-[^{18}F]**8** and (*R*)-[^{18}F]**8** showed a peak tumor uptake of radioactivity within 7 min p.i. for both enantiomers. After the initial few min, which is dominated by flow, the tumor uptake of (*S*)-[^{18}F]**8** was higher than (*R*)-[^{18}F]**8**. Furthermore, the tumor uptake of (*S*)-[^{18}F]**8** was relatively constant during the study with only 10% washout whereas the tumor uptake with (*R*)-[^{18}F]**8** decreased by approximately 50% over the course of the study. At 45-60 min p.i., the average SUV was 0.83 ± 0.14 for *S*-[^{18}F]**8** compared to 0.49 ± 0.07 for (*R*)-[^{18}F]**8** ($p < 0.05$). In the normal brain, the average SUVs were similar for both enantiomers over time with slightly higher activity observed with (*S*)-[^{18}F]**8** compared to (*R*)-[^{18}F]**8**; this did not reach statistical significance. Overall, both enantiomers demonstrated good tumor imaging properties, which was consistent with the biodistribution studies. Together, these data suggest that (*S*)-[^{18}F]**8** is the superior enantiomer for imaging due to higher tumor and brain uptakes at early and late time points and better retention in the tumor over time.

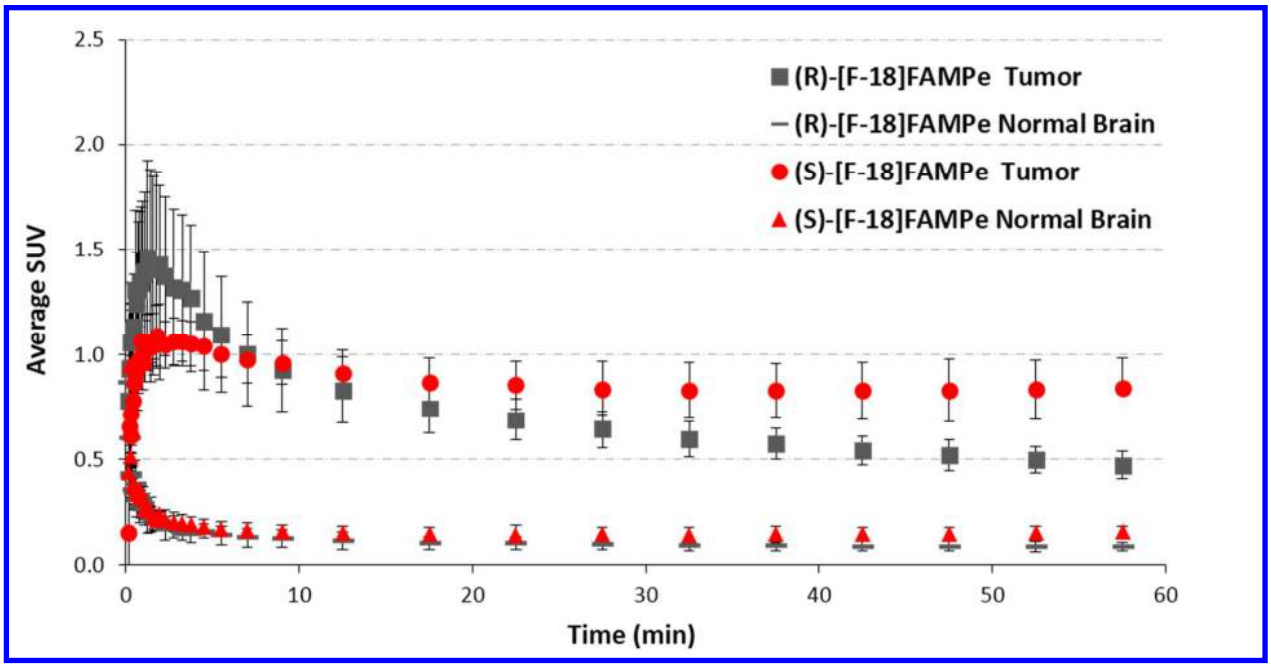

Figure 6: Time-activity curves of (*S*)-[^{18}F]**8** and (*R*)-[^{18}F]**8** uptake in intracranial DBT tumors and contralateral normal brain. Mice were anesthetized with 1% isoflurane/oxygen for 0-60 min dynamic microPET/CT scans.

Intravenous injection of 150-200 μCi (5.55-7.4 MBq) of (*S*)-[^{18}F]**8** was done on day 14 and (*R*)-[^{18}F]**8** on day 15 post unilateral tumor implantation. The same animals were used for imaging both tracers. The data are displayed as average SUVs, and each time point represents the mean of 4 animals.

In **Figure 7**, tumor to brain ratios of the two new enantiomers (*S*)-[^{18}F]**8** and (*R*)-[^{18}F]**8** measured with small animal PET at 45-60 min after injection are compared with those obtained with the system L substrate (*S*)-[^{18}F]FET and the system A substrate (*R*)-[^{18}F]MeFAMP. The data show that (*S*)-[^{18}F]**8**, and (*R*)-[^{18}F]**8** had higher tumor to brain ratio compared to (*S*)-[^{18}F]FET ($p < 0.001$ for both enantiomers) but lower than (*R*)-[^{18}F]MeFAMP ($p < 0.001$ for both enantiomers). These findings suggest that (*S*)-[^{18}F]**8** and (*R*)-[^{18}F]**8** could provide better tumor visualization and a larger dynamic range for monitoring response to therapy than (*S*)-[^{18}F]FET. However, for (*S*)-[^{18}F]**8** and (*R*)-[^{18}F]**8** and even more for (*R*)-[^{18}F]MeFAMP, the high tumor to brain ratios obtained are due primarily to low brain uptake which could decrease visualization of non-enhancing regions within gliomas. Conventional orthotopic models of high grade gliomas have disrupted BBBs in tumor tissue which limits their predictive value for the visualization of non-enhancing tumor regions that are often encountered in human gliomas. Longer chain analogues of (*S*)-[^{18}F]**8** are expected to show enhanced system L transport and may prove superior to (*S*)-[^{18}F]**8** for imaging the non-enhancing regions of brain tumors. Representative PET/CT images of (*S*)-[^{18}F]**8** are shown in **Figure 8**. The amount of activity in the bone observed in the small animal PET studies was less than expected based on the biodistribution studies. The reason for this difference is not clear but may be due to effects of anesthesia during the small animal PET studies.

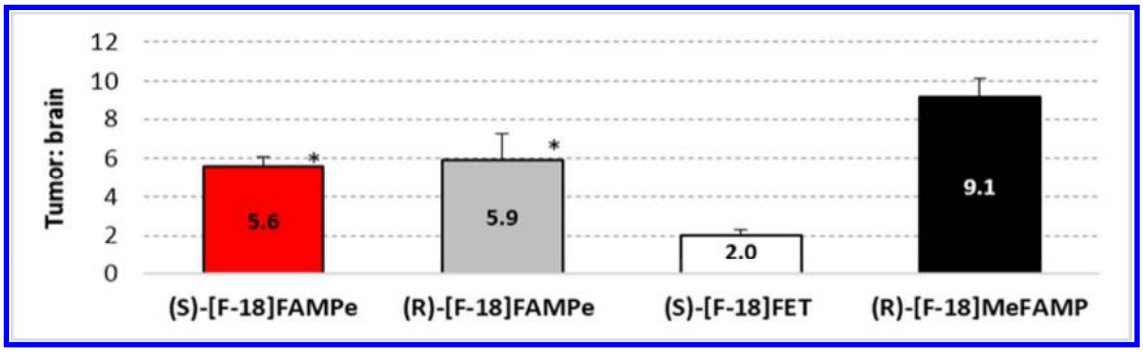

Figure 7: Tumor to brain ratios from small animal PET studies performed with (*S*)-[^{18}F]**8** and (*R*)-[^{18}F]**8** in the same animals (n= 4), and with (*S*)-[^{18}F]FET and (*R*)-[^{18}F]MeFAMP (n= 3) approximately 45-60 min after injection. SUV-Tumor (*S*)-[^{18}F]FAMPe = 0.83 ± 0.14, SUV-Brain (*S*)-[^{18}F]FAMPe = 0.15 ± 0.03, SUV-Tumor (*R*)-[^{18}F]FAMPe = 0.49 ± 0.07, SUV-Brain (*R*)-[^{18}F]FAMPe = 0.09 ± 0.02, SUV-Tumor (*S*)-[^{18}F]FET = 1.10 ± 0.09, SUV-Brain (*S*)-[^{18}F]FET = 0.55 ± 0.05, SUV-Tumor (*R*)-[^{18}F]MeFAMP = 0.77 ± 0.23, SUV-Brain (*R*)-[^{18}F]MeFAMP = 0.09 ± 0.02. Errors bars show SD. *p*-Values represent comparisons of the tumor: brain ratios for both radiotracers, (*S*)-[^{18}F]**8** and (*R*)-[^{18}F]**8**, with (*S*)-[^{18}F]FET and with (*R*)-[^{18}F]MeFAMP through 1-way ANOVA with Tukey post-tests. * = $p < 0.001$.

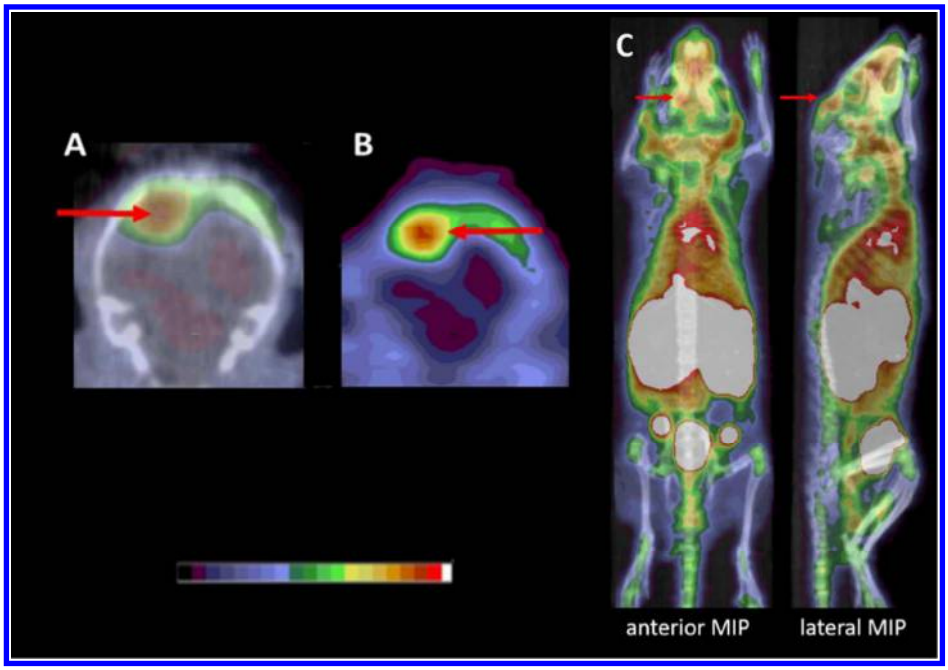

Figure 8: Representative (*S*)-[^{18}F]**8** small animal PET/CT (A) and PET (B) images of a mouse with an intracranial DBT gliomas (red arrows) acquired 45-60 min after injection of tracer. Additional tumor tracking with less intense tracer uptake is seen tracking along the skull. (C) Anterior and lateral maximum intensity projection (MIP) PET/CT

images obtained 50-60 min after injection of (*S*)-[^{18}F]**8**. The intracranial DBT tumor is designated by the red arrow and is better seen on the lateral MIP due to the lack of obscuring salivary and nasopharyngeal activity.

Conclusion

Both enantiomers of a novel α,α-disubstituted fluorinated amino acid, (*S*)- and (*R*)-[^{18}F]**8**, were prepared through efficient organic and radiosyntheses. Both tracers have promising imaging properties with (*S*)-[^{18}F]**8** displaying superior properties compared to the (*R*)-enantiomer in the mouse DBT glioma model. In vitro cell uptake assays demonstrated that (*S*)- and (*R*)-[^{18}F]**8** enter DBT cells via multiple transport systems including system L and other neutral amino acid transporters but not through system A transport. Additionally, the uptake of (*S*)-[^{18}F]**8** was inhibited by L-glutamine to a greater extent than the (*R*)-enantiomer. Biodistribution studies in a mouse subcutaneous DBT model of glioblastoma demonstrated higher and more persistent tumor uptake with (*S*)-[^{18}F]**8** than with the (*R*)-enantiomer. Small animal PET imaging showed that (*S*)-[^{18}F]**8** had rapid and persistent intracranial tumor uptake with contralateral normal brain uptake greater than the system A tracer (*R*)-[^{18}F]MeFAMP but less than the system L tracer (*S*)-[^{18}F]FET. Overall (*S*)-[^{18}F]**8** is a promising new tracer for tumor imaging and may serve as a lead compound for optimized system L and glutamine transport imaging agents.

Experimental Section

Materials and Instrumentation. All reagents and materials were purchased from commercially available sources. Chemicals were purchased from Aldrich Chemicals Co. (Milwaukee, WI USA), Sigma Chemical Co. (St Louis, Mo USA) and from Advanced Chemtech Co. (Louisville, KY USA), and solvents were purchased from Aldrich Chemicals and Products (Pittsburg, PA USA). Chromatography was carried out using silica gel 60 (0.040-0.063 mm) from EMD Millipore. Thin-layer chromatography (TLC) analyses were performed with 200μm UV254 silica gel backing on aluminum sheets (EMD Millipore USA). The

TLC plates were revealed with ninhydrin and/or iodide stains. Sep-Pak C18 Plus Short Cartridge and Oasis HLB Plus Light cartridge were purchased from Waters, Inc. (Milford, MA USA). Dionex OnGuard II A cartridge was purchased from Fisher Scientific (Pittsburgh, PA). Melting points were measured with an IA9100X1 Series digital melting point apparatus (ThermoFisher Scientific, USA) in capillary tubes and are uncorrected. ^{1}H and ^{13}C NMR spectra were recorded either on a 300 MHz or 400 MHz NMR spectrometer (Varian/Agilent, Santa Clara, USA) maintained by the Washington University High Resolution NMR Facility. Chemical shifts (δ values) are reported as parts per million (ppm) and coupling values are reported in Hertz. Elemental analyses, performed by Atlantic Microlabs, Inc. (Norcross, GA USA), were conducted on non-radioactive new intermediates synthesized during the multistep synthesis and were within 0.4% of theoretical values with the exception of the non-radioactive hydrochloric acid salt of the fluorinated amino acid (compound (*R*,*S*)-**8**). The purity of (*R*,*S*)-**8** was determined based on HPLC analysis and was higher than 95%. This non-radioactive compound was only used as an HPLC standard for confirming the identity of the ^{18}F-labeled target compounds but not for biological studies. The purity of the final ^{18}F-labeled amino acids used for biological studies was measured using radiometric TLC and HPLC and met the requirements of 95% or greater purity. For the compounds whose purity was determined by analytical HPLC, the Chirex 3126 D-penicillamine column (15 cm × 4.6 mm) was used with a solution of 85% 3 mM copper sulfate ($CuSO_4$): 15% acetonitrile as mobile phase, a flow rate of 1 mL/min, a detection at λ= 254 nm, a column temperature of 25 °C. For compound (*R*,*S*)-**8**, 10 µl of a 10.8 mM solution was injected. Mass spectra were run on a Bruker Maxis Q-ToF mass spectrometer using high-resolution electron ionization and were carried out at the Chemistry Department of Washington University in St Louis. Statistical analyses were performed using GraphPad Prism software (GraphPad Software, La Jolla, CA) with p-values of 0.05 or less considered statistically significant.

Chemistry. *Tert-butyl (S)-2-((diphenylmethylene)amino)propanoate* (*S*)-**1**. Benzophenone imine (2.77 mL, 16.51 mmol) was added to a solution of L-(*S*)-alanine *tert*-butyl ester hydrochloride (3 g, 16.51 mmol) in 30 mL DCM. The mixture was stirred at rt for 2 h. A white precipitate was formed. The mixture was diluted with water and two phases were separated. The aqueous phase was extracted with DCM (2 × 30 mL). The combined organic layers were washed with brine (1 × 45 mL), dried over sodium sulfate (Na_2SO_4), filtered and finally concentrated to dryness under reduced pressure. (*S*)-**1** was obtained as a colorless oil (94%) which was used without further purification.[44]

^{1}H NMR ($CDCl_3$): δ 1.40 (d, *J*= 6.7Hz, 3H), 1.45 (s, 9H), 4.03 (q, *J*= 6.7Hz, 1H), 7.18-7.20 (m, 2H), 7.30-7.48 (m, 6H), 7.63-7.65 (m, 2H). ^{1}H NMR spectrum agrees with literature report.[45]

^{13}C NMR ($CDCl_3$): 19.3 (CH_3), 28.1 ($3CH_3$), 61.4 (CH), 80.8 (C), 127.8 (2CH), 128.1 (2CH), 128.6 (2CH), 128.8 (2CH), 130.3 (2CH), 136.7 (C), 139.8 (C), 169.4 (C=N), 172.1 (C=O).

Tert-butyl (R,S)-2-((diphenylmethylene)amino)-2-methylpent-4-enoate (*R*,*S*)-**2**. Imine **1** (500 mg, 1.61 mmol) solubilized in 1 mL THF was added to a solution of LDA (1.77 mL of 2.0 M solution in THF, heptane, ethylbenzene, 3.54 mmol) in 6 mL anhydrous THF at -78 °C under nitrogen. An orange enolate solution resulted. The mixture was stirred at -78 °C for 1 h, and then the alkylating agent allyl iodide (0.33 mL, 3.54 mmol) was added. The solution was stirred for overnight and allowed to return to rt. The reaction was quenched with the addition of a saturated solution of ammonium chloride (NH_4Cl) (10 mL) and diluted with diethyl ether (Et_2O) (15 mL). Two phases were separated. The aqueous phase was extracted with Et_2O (2 × 15 mL). The combined organic layers were washed with brine (1 × 20 mL), dried over Na_2SO_4, filtered and concentrated to dryness under reduced pressure. The crude compound was purified on silica gel column chromatography eluted with 20% ethyl acetate in hexane to give (*R*,*S*)-**2** as a colorless oil (90%).

^{1}H NMR ($CDCl_3$): δ 1.24 (s, 3H), 1.30 (s, 9H), 2.59-2.69 (m, 2H), 5.10-5.14 (m, 2H), 5.96-6.07 (m, 1H), 7.20-7.37 (m, 8H), 7.54-7.56 (m, 2H).

^{13}C NMR ($CDCl_3$): 24.5 (CH_3), 28.1 ($3CH_3$), 48.1 (CH_2), 66.7 (C), 80.9 (C), 117.9 (CH_2=), 128.0 (4CH), 128.4 (CH), 128.7 (2CH), 128.9 (2CH), 129.9 (CH), 130.2 (CH), 138.6 (C), 141.8 (C), 167.1 (C=N), 173.6 (C=O).

HRMS (ESI): m/z calculated for $C_{23}H_{27}NO_2$ + H [M + H]+: 350.2115. Found: 350.2126.

Tert-butyl (R,S)-2-amino-2-methylpent-4-enoate (*R*,*S*)**-3**. Hydroxylamine hydrochloride (897 mg, 12.91 mmol) was added to a solution of **2** (1.29 g, 3.69 mmol) in 30 mL anhydrous methanol under nitrogen at rt. After 1 hour, the reaction was complete. The mixture was then concentrated under reduced pressure. Water (30mL) and DCM (60 mL) were added and the two phases were separated. The aqueous phase was basified to pH=7.5 by using a saturated solution of potassium carbonate (K_2CO_3), then extracted with DCM (2 × 40 mL). The combined organic layers were washed with brine (40 mL), dried over Na_2SO_4, filtered, and concentrated to dryness under reduced pressure. The crude compound was purified on silica gel column chromatography; it was eluted first with 20% ethyl acetate in hexane then with 10% methanol in DCM to provide the free amine (*R*,*S*)**-3** as a colorless oil (65%).

^{1}H NMR ($CDCl_3$): δ 1.29 (s, 3H), 1.46 (s, 9H), 1.93 (bs, 2H), 2.21-2.26 (m, 1H), 2.46-2.52 (m, 1H), 5.11-5.16 (m, 2H), 5.67-5.78 (m, 1H).

^{13}C NMR ($CDCl_3$): δ 26.5 (CH_3), 28.1 ($3CH_3$), 45.3 (CH_2), 57.6 (C), 81.0 (C), 119.2 (CH_2=), 133.2 (CH=), 176.6 (C=O). NMR spectrums agree with literature report.[46]

Tert-butyl (R,S)-2-((tert-butoxycarbonyl)amino)-2-methylpent-4-enoate (*R*,*S*)**-4**. Compound **3** (227 mg, 1.22 mmol) was solubilized in 10 mL THF, then di-*tert*-butyl dicarbonate (532 mg, 2.44 mmol) was added and the solution was stirred at rt overnight. Brine (20 mL) and DCM (40 mL) were added and the two phases were separated. The aqueous phase was extracted with DCM (2 × 40 mL). The combined organic layers were dried over Na_2SO_4, filtered, and concentrated to dryness under reduced pressure. The

crude compound was purified on silica gel column chromatography; it was eluted first with 100% hexane then with 10% ethyl acetate in hexane to provide the protected amine (*R*,*S*)-**4** as a colorless oil (92%).

^{1}H NMR ($CDCl_3$): δ 1.42 (s, 9H), 1.45 (s, 9H), 1.50 (s, 3H), 2.48-2.53 (m, 1H), 2.77 (bs, 1H), 5.08-5.12 (m, 2H), 5.28 (bs, 1H), 5.61-5.72 (m, 1H).

^{13}C NMR ($CDCl_3$): δ 23.4 (CH_3), 28.0 ($3CH_3$), 28.5 ($3CH_3$), 41.3 (CH_2), 59.3 (C), 81.8 (2C), 119.1 (CH_2=), 132.8 (CH=), 154.4 (C=O), 173.2 (C=O).

HRMS (ESI): m/z calculated for $C_{15}H_{27}NO_4$ + Na [M + Na]: 308.1832. Found: 308.1835.

Elemental analysis calculated (%) for $C_{15}H_{27}NO_4$: C 63.13, H 9.54, N 4.91. Found: C 63.13, H 9.60, N 4.99.

Tert-butyl (R,S)-2-((tert-butoxycarbonyl)amino)-5-hydroxy-2-methylpentanoate (*R*,*S*)-**5**. Borane-THF solution (10.88 mL of 1.0 M solution, 10.88 mmol) was slowly added to a solution of **4** (840 mg, 2.94 mmol) in 60 mL anhydrous THF under nitrogen at 0 °C. The resulting solution was stirred for 2 hours at 0 °C. Then, still at 0 °C, a solution of 1 M sodium hydroxide (NaOH) (10.88 mL, 10.88 mmol) was added slowly, followed by aqueous hydrogen peroxide 30% (4.60 mL, 40.26 mmol). The mixture was stirred overnight and allowed to return to rt. Ethyl acetate (100 mL) and brine (100 mL) were added, and the two layers were separated. The aqueous phase was extracted with ethyl acetate (2 × 150 mL). The combined organic layers were dried over Na_2SO_4, filtered and concentrated to dryness under reduced pressure. The crude compound was purified on silica gel column chromatography eluted with 40% ethyl acetate in hexane to give (*R*,*S*)-**5** as a white solid (62%). mp: 94-95 °C

^{1}H NMR ($CDCl_3$): δ 1.41 (s, 9H), 1.45 (s, 9H), 1.49 (s, 3H), 1.51-1.86 (m, 3H), 2.14 (bs, 1H), 3.61 (t, *J*= 6.3Hz, 2H), 5.43 (bs, 1H).

^{13}C NMR ($CDCl_3$): δ 23.7 (CH_3), 27.5 (CH_2), 28.0 ($3CH_3$), 28.5 ($3CH_3$), 32.9 (CH_2), 59.6 (C), 62.7 (CH_2), 81.9 (2C), 154.5 (C=O), 173.7 (C=O).

HRMS (ESI): m/z calculated for $C_{15}H_{29}NO_5$ + Na [M + Na]: 326.1938. Found: 326.1941.

Elemental analysis calculated (%) for $C_{15}H_{29}NO_5$: C 59.38, H 9.63, N 4.62. Found: C 59.39, H 9.72, N 4.63.

Tert-butyl (R,S)-2-((tert-butoxycarbonyl)amino)-2-methyl-5-(tosyloxy)pentanoate (*R*,*S*)**-6**. Sodium *tert*-butoxide (132mg, 1.37mmol) was added to a solution of the alcohol **5** (347 mg, 1.14 mmol) and *p*-toulenesulfonyl chloride (326 mg, 1.71 mmol) in 12 mL anhydrous DCM at 0 °C and under nitrogen. After 5 min of stirring at 0 °C, the ice bath was removed, and the reaction was stirred overnight at rt. The mixture was then concentrated under reduced pressure, and the crude product was purified on silica gel column chromatography eluted with 10% ethyl acetate in hexane to provide (*R*,*S*)**-6** as a white solid (40%). mp: 59-61 °C

^{1}H NMR ($CDCl_3$): δ 1.38 (s, 9H), 1.42 (s, 12H), 1.47-1.65 (m, 2H), 1.74-2.00 (m, 1H), 2.04-2.10 (m, 1H), 2.43 (s, 3H), 3.90-4.02 (m, 2H), 5.34 (bs, 1H), 7.32 (d, *J*= 8.4Hz, 2H), 7.75 (d, *J*= 8.4Hz, 2H).

^{13}C NMR ($CDCl_3$): δ 21.7 (CH_3), 24.2 (CH_3), 27.8 ($3CH_3$), 28.4 ($3CH_3$), 29.8 (CH_2), 32.2 (CH_2), 59.3 (C), 70.4 (CH_2), 82.1 (2C), 127.9 (2CH), 129.9 (2CH), 132.9 (C), 144.9 (C), 154.1 (C=O), 173.2 (C=O).

HRMS (ESI): m/z calculated for $C_{22}H_{35}NO_7S$ + Na [M + Na]: 480.2026. Found: 480.2032.

Elemental analysis calculated (%) for $C_{22}H_{35}NO_7S$: C 57.75, H 7.71, N 3.06. Found: C 57.89, H 7.69, N 3.06.

Tert-butyl (R,S)-2-((tert-butoxycarbonyl)amino)-5-fluoro-2-methylpentanoate (*R*,*S*)**-7**. Cesium fluoride (198 mg, 1.70 mmol) was added to a solution of the tosylate **6** (155 mg, 0.34 mmol) in 1.5 mL anhydrous 2-methylbutan-2-ol. The mixture was stirred at 100 °C for 1 hour. Then, the reaction mixture was triturated with ethyl ether to remove most of the ionic salts. The filtrate was concentrated under reduced pressure and the crude product was purified on silica gel column chromatography and eluted with 8% ethylacetate in hexane to provide (*R*,*S*)**-7** as a white solid (34%). mp: 69-71 °C

^{1}H NMR ($CDCl_3$): δ 1.41 (s, 9H), 1.44 (s, 9H), 1.50 (3H), 1.52-1.82 (m, 2H), 1.84-1.92 (m, 1H), 2.20 (bs, 1H), 4.29-4.40 (m, 1H), 4.41-4.51 (m, 1H), 5.40 (bs, 1H).

^{13}C NMR ($CDCl_3$): δ 23.6 (CH_3), 25.6 (d, ^2J (C,F)= 20.2Hz, CH_2), 27.9 ($3CH_3$), 28.5 ($3CH_3$), 32.2 (CH_2), 59.5 (C), 82.0 (2C), 83.8 (d, ^1J (C,F)= 165.6Hz, CH_2F), 154.2 (C=O), 173.5 (C=O).

HRMS (ESI): m/z calculated for $C_{15}H_{28}FNO_4$ + Na [M + Na]: 328.1895. Found: 328.1897.

Elemental analysis calculated (%) for $C_{15}H_{28}FNO_4$: C 58.99, H 9.24, N 4.59. Found: C 58.88, H 9.24, N 4.53.

(R,S)-2-amino-5-fluoro-2-methylpentanoic acid hydrochloride (*R*,*S*)**-8**. The protected amino acid **7** (21 mg, 0.069 mmol) was stirred in 0.3-0.4 mL of 4 M hydrochloric acid (HCl) at 60 °C for 90 min. The mixture was then concentrated under reduced pressure. The residue obtained was triturated in Et_2O to precipitate the desired compound. After filtration, product **8** was obtained as a white solid (78%). mp: 172-173 °C

^{1}H NMR (D_2O): δ 1.60 (s, 3H), 1.64-2.14 (m, 4H), 4.46 (dt, ^2J (H,F)= 47.0Hz, ^3J (H,H)= 5.7Hz, 2H).

^{13}C NMR (D_2O): δ 21.6 (CH_3), 24.1 (d, ^2J (C,F)= 20.1Hz, CH_2), 32.6 (CH_2), 59.8 (C), 83.9 (d, ^1J (C,F)= 166.8Hz, CH_2F), 174.1 (C).

HRMS (ESI): m/z calculated for $C_6H_{13}FNO_2$ - Cl [M - Cl]: 150.0925. Found: 150.0926.

Di-tert-butyl (R,S)-2-methylpyrrolidine-1,2-dicarboxylate, (*R*, *S*)**-9**. This compound is a side product of reaction providing (*R*, *S*)**-7**. It was obtained as a white solid (56%). NMR analysis showed two sets of signals corresponding to the two conformational isomers.

^{1}H NMR ($CDCl_3$): δ 1.42 (s, 3.3H), 1.43 (s, 5.7H), 1.43 (s, 3.3H), 1.44 (s, 5.7H), 1.47 (s, 1.9H), 1.49(s, 1.1H), 1.74-1.92 (m, 3H), 2.02-2.16 (m, 1H), 3.43 (t, 0.7H, *J*= 6.5Hz), 3.47-3.58 (m, 1.3H).

^{13}C NMR ($CDCl_3$): δ 22.3, 22.7, 23.3, 23.5, 28.0, 28.1, 28.5, 28.6, 39.3, 40.9, 48.2, 48.2, 65.2, 65.7, 79.2, 79.9, 80.4, 80.7, 153.9, 173.8, 173.9. NMR spectrums agree with literature report.[47]

(R)- or (S)-2-((tert-butoxycarbonyl)amino)-2-methylpent-4-enoic acid, (*R*)-**10** *or* (*S*)-**10**. The respective starting material (*S*)-(-)-α-allylalanine or (*R*)-(+)-α-allylalanine (500 mg, 3.87 mmol) was suspended in 11 mL methanol-triethylamine-1 N NaOH (9/1/1: v/v/v) and di-*tert*-butyl dicarbonate (1.69 g, 7.74 mmol) was added in one portion. The reaction was stirred at rt overnight. The organic solvent was removed under reduced pressure, and 10 ml of ethyl acetate was added. The pH of the aqueous phase was adjusted to 2 with 3 N HCl. The organic layer was retained while the aqueous layer was saturated with sodium chloride and extracted with ethyl acetate (3 × 10 mL). The combined organic phases were dried over sodium sulfate, filtered, and concentrated to dryness under reduced pressure. The respective product (*R*)-**10** or (S)-**10** was obtained as a colorless oil (88 and 89% respectively) which was used without further purification.

^{1}H NMR ($CDCl_3$): δ 1.44 (s, 9H), 1.54 (s, 3H), 1.44 (s, 9H), 1.54 (s, 3H), 2.61-2.75 (bm, 2H), 5.14-5.18 (m, 2H), 5.68-5.78 (m, 1H), NH and COOH were not observed.

^{13}C NMR ($CDCl_3$): δ 23.3 (CH_3), 28.4 ($3CH_3$), 41.4 (CH_2), 59.1 (C), 77.4 (C), 120.1 (CH_2), 132.07 (CH), 155.4(C), 178.2 (C). NMR spectrums agree with literature report.[48]

Radiochemistry. [^{18}F]-fluoride was produced using an RDS-11 cyclotron in the Washington University Cyclotron Facility. [^{18}F]fluoride was produced from [^{18}O]water and the ^{18}O(p,n)^{18}F reaction. Typical radiosyntheses used approximately 50 mCi of [^{18}F]fluoride. First, the [^{18}F]fluoride was dried by azeotropic distillation using acetonitrile (2 × 1 mL then 2 × 0.5 mL) in the presence of potassium carbonate (0.5 mg in 25 μL water) and Kryptofix 2.2.2 ($K_{2.2.2}$) (3 mg in 50 μL anhydrous acetonitrile) between 96 and 105 °C under a flow of nitrogen. Then, a solution of the respective tosylate precursor (*S*)-**6** or (*R*)-**6** (5 mg in 500 μL of anhydrous 2-methylbutan-2-ol) was added, and the mixture was heated for 10 min between 96 and 105 °C in a sealed vessel. Incorporation of [^{18}F]fluoride was estimated using radiometric thin layer chromatography (radio-TLC), the elution was done in 100% ethyl acetate. Then, ~

8 mL water was added to the mixture and the solution was passed through a Sep-Pak C18 Plus Short cartridge which trapped the intermediate (*S*)-[^{18}F]**7** or (*R*)-[^{18}F]**7**. The C18 cartridge was rinsed with 2 × 8 mL water. The crude ^{18}F-intermediate was eluted with acetonitrile (3 × 0.5 mL), water was added (1.5 mL) and the eluent was purified using an Agilent Zorbax SB-C18 semipreparative high-performance liquid chromatography (HPLC) column (25 cm × 4.6 mm × 5 μm) eluted with a gradient mobile phase: solution A (30% acetonitrile, 70% water, 0.1% trifluoroacetic acid) and solution B (80% acetonitrile, 20% water, 0.1% trifluoroacetic acid) starting from 70% solution A, 30% solution B and transitioning to 100% solution B in 30 min, with a flow rate of 4 mL/min and λ= 230nm. In these conditions, intermediates (*S*)-[^{18}F]**7** and (*R*)- [^{18}F]**7** had a retention time of 21-22 min. The intermediate HPLC eluent was diluted with ~ 40 mL water, and passed through an Oasis HLB Plus Light cartridge; after 2 more washes, (*S*)-[^{18}F]**7** or (*R*)-[^{18}F]**7** was eluted with very small amount of ethanol (about 300 μl). Then, 500 μL of a solution of hydrochloric acid 1 M was added, and the mixture was heated for 12 min between 96 and 105 °C to provide the desired product (*S*)-[^{18}F]**8** or (*R*)-[^{18}F]**8**. After cooling, the solution was diluted in 0.5 ml sterile water and passed through a Dionex OnGuard II A cartridge, the process was repeated three times. Finally, the final product (*S*)-[^{18}F]**8** or (*R*)-[^{18}F]**8** was obtained in pH= 6 and in a form suitable for cell uptake studies. For the animal studies, the final product was formulated in a 0.9% saline solution. The final products identities as well as the radiochemical and enantiomeric purity were assessed by coinjection of the racemic non-radioactive standard (*R,S*)-**8** and the (*S*)-[^{18}F]**8** or (*R*)-[^{18}F]**8** onto a chiral analytical column: the Chirex 3126 D-penicillamine column (15 cm × 4.6 mm) using a solution of 85% 3 mM $CuSO_4$: 15% acetonitrile as mobile phase with a flow rate of 1 mL/min and λ= 254nm. The specific activity was also determined by using that column and those conditions. The mass associated with ^{18}F-labeled product was determined by comparison of the intregrated UV absorbance with a calibrated mass/UV absorbance standard curve of the racemic non-radioactive standard (*R,S*)-**8**.

(*R*)-[^{18}F]MeFAMP was radiosynthesized in two steps from a cyclic sulfamidate precursor using the method described by Yu et al..[31] (*S*)-[^{18}F]FET was radiosynthsized using the method described by

Zuhayra et al. starting from 2-bromoethyl triflate as precursor which reacts with [^{18}F]fluoride to provide 1-bromo-2-^{18}F-fluoroethane which in turn used for the (*O*)-alkylation of the L-tyrosine.[49]

Cell Uptake assays.

Cell uptake assays were performed using the cluster tray method as reported in the literature.[29] Mouse DBT glioma cells were cultured at 1×10^5 per 24 wells (Corning, NY, USA) for 48 hours in a 5% carbon dioxide atmosphere in 10% fetal bovine serum (FBS) DMEM culture medium. Two buffer conditions with and without sodium were used for the assays. The phosphate-buffered saline solution contained 105 mM sodium chloride, 3.8 mM potassium chloride, 1.2 mM potassium bicarbonate, 25 mM sodium phosphate dibasic, 0.5 mM calcium chloride dehydrate, 1.2 mM magnesium sulfate, and 5.6 mM D-glucose. The sodium-free phosphate-buffered choline solution was identical to the phosphate-buffered saline solution except choline chloride and choline phosphate dibasic were substituted for sodium chloride and sodium phosphate dibasic, respectively.

The following inhibitors were used for the cell uptake assays: *N*-methyl-α-aminoisobutyric acid (MeAIB, 10 mM), a mixture of L-alanine/L-serine/L-cysteine (ASC, 3.3 mM of each amino acid to make the 10 mM solution, or 0.33 mM of each amino acid to make the 1 mM solution), (*R*,*S*)-(endo, exo)-2-aminobicyclo(2,2,1)-heptane-2-carboxylic acid (BCH, 10 mM), and finally L-glutamine (0.1 mM, 1 mM, or 10 mM). The control conditions contained 10 mM of sucrose to maintain consistent osmolality. The assays were performed as described previously at pH 7.40 with each condition performed in 4 or 8 replicates. Briefly, cells were washed twice with 37 °C assay buffer (2 mL) prior to initiating the assay. For each of the four tracers: (*S*)-[^{18}F]**8** and (*R*)-[^{18}F]**8**, (*R*)-[^{18}F]-MeFAMP, and (*S*)-[^{18}F]FET, solutions containing approximately 2.0 mCi/mL (64 MBq/mL) were prepared in the appropriate assay buffer, then 20 μL of the tracer was added to appropriate buffer with or without inhibitors. Cells were incubated with radiotracers in assay buffer (0.4 mL total volume) under control or inhibitor conditions for 30 seconds at 37 °C. The assay buffer was then discarded from each well followed by washes (3 × 2 mL) ice-cold

buffer to remove extracellular radiotracer. The cells were lysed with 0.2% sodium dodecyl sulfate (SDS)/0.2 M sodium hydroxide (0.3 mL) at rt for 30 min. A 100 μL portion of the lysate from each well was counted to determine the amount of radioactivity taken up by the cells, and 3 × 20 μL portions were used for determination of protein content using the bicinchoninic acid (BCA) method (Pierce, BCA Protein Assay Kit). Standard dilutions of each assay condition were counted to determine the amount of activity added to each well. The amount of radioactivity per well was normalized based on the amount of radioactivity added and the protein content of each cell. The uptake data were expressed as percent of uptake relative to control, and each plate was analyzed with a one-way analysis of variance (ANOVA) with Dunnett's multiple comparison post-tests. The choline sucrose control condition was compared to the choline BCH condition using a 2-sided t-test.

DBT Tumor model

All animal experiments were conducted following the Institutional Animal Care and Use Committee-approved protocols in compliance with the Guide for the Care and Use of Research Animals. For the unilateral intracranial tumors, mouse DBT tumor cells (1×10^4 cells suspended in a volume of 8 μL) were implanted in the right mid cerebrum of male BALB/C mice (24-26 g) as described previously.[34, 50] For subcutaneous tumors, the DBT cells (5×10^5 cells suspended in a volume of 50 μL) were injected subcutaneously into the flanks of male BALB/c mice (23-30 g).[38] Tumor-bearing animals were used for imaging and biodistribution studies 14 - 15 days after implantation.

Biodistribution studies with (*S*)- and (*R*)-[^{18}F]8 in BALB/c mice with subcutaneous DBT glioma.

The same procedure was used to evaluate the biodistribution of (*S*)-[^{18}F]**8** and (*R*)-[^{18}F]**8** in tumor-bearing mice. 23 μCi (0.85 MBq) of (*S*)-[^{18}F]**8** or 29 μCi (1.07 MBq) of (*R*)-[^{18}F]**8** was administrated via tail vein injection in conscious animals. Groups of five animals were euthanized at 5, 30, and 60 min post-injection. The tumor and tissues of interest were collected, weighed and the radioactivity was measured

using an automated Beckman Gamma 8000 well counter with a standard dilution of the injectate. The raw counts were decay-corrected, and the counts were normalized as the percent of total injected dose per gram of tissue (%ID/g). For each tracer at each time point, the tumor uptake versus normal brain uptake was compared using 2-tailed paired t-tests. Uptake data for (*S*)- versus (*R*)-[^{18}F]**8** in tumor and brain tissue were compared separately at all-time points through 1-way ANOVA with Tukey post-tests.

Small animal PET/CT studies in mice with intracranial DBT tumors

Male BALB/c mice (n= 4) with unilateral intracranial DBT tumors were placed in an induction chamber containing ~2% isoflurane/oxygen then secured to a custom double bed for placement of tail vein catheters; anesthesia was maintained via nose-cone at ~1% isoflurane/oxygen for the imaging procedures. The mice underwent dynamic small animal PET imaging from 0 to 60 min after intravenous tail injection of 150-200 μCi (5.55-7.4 MBq) of (*R*)-[^{18}F]**8** on day 14 and (*S*)-[^{18}F]**8** on day 15, using INVEON and MicroPET Focus 220 systems (Siemens Medical Solutions Inc.). Computed Tomography (CT) images were acquired with the INVEON system on all mice. At the conclusion of the imaging studies, the animals were euthanized, and their brains were fixed in 4% paraformaldehyde for histologic analysis with hematoxylin and eosin staining to verify the presence and location of tumor. The small animal PET data were analyzed by manually drawing 3-dimensional regions of interest (ROIs) over the areas of tumor identified on the PET studies. ROIs for normal brain were drawn over the cerebral hemisphere contralateral to the tumor. These data generated time activity curves (TACs). The uptake data were expressed as average standardized uptake values (SUVs) for each ROI. The average of the SUVs in brain and tumor, as well as the average of the tumor: brain ratios at 45-60 min post-injection for both enantiomer of [^{18}F]**8** were compared through 1-way ANOVA with Tukey post-tests. The tumor:brain ratios obtained with (*S*)-[^{18}F]**8**, (*R*)-[^{18}F]**8**, (*R*)-[^{18}F]MeFAMP, and (*S*)-[^{18}F]FET were compared through 1-way ANOVA with Tukey post-tests.

Associated content:

Supporting information:

The data of the biodistribution study on mice with subcutaneous DBT tumors in **Table 1** are shown as a bar graph representation. This material is available free of charge via the Internet at http://pubs.acs.org

Author information:

Corresponding author:

*Email: mcconathyj@mir.wustl.edu. Phone: (314) 362-2809. Fax: (314)362-8555.

Acknowledgments

We are grateful to the assistance of the personnel of the Washington University Cyclotron Facility for [^{18}F]fluoride production. This research was supported through grants from the National Cancer Institute (K08CA154790) and Department of Energy (SC0004832). We thank also the Siteman Cancer Center Small Animal Imaging Core for the use of the Pre-Clinical PET/CT Imaging Facility, which provided biodistribution and small animal PET/CT services. The Siteman Cancer Center is funded in part through the National Cancer Institute (P50CA094056). The Siemens Inveon scanner was acquired through an NIH High-End Instrumentation grant (S10 RR 025097).

We would like to thank the Department of Chemistry staff and the Washington University High Resolution NMR Facility for assistance with NMR spectra; purchase of the 400 MHz NMR instrument was partially supported by S10 RR027207 from the NIH Shared Instrument Grant program. The mass spectral data from Washington University Mass Spectrometry Resource were supported by grants from

the National Institute of General Medical Sciences (8 P41 GM103422-35) from the National Institutes of Health.

Abbreviations used:

PET, positron emission tomography; DBT, delayed brain tumor; CT, computed tomography; CsF, cesium fluoride; HLB, hydrophilic-lipophilic-balanced; EOS, end of synthesis; ID, injected dose; p.i., injected dose; SUV, standardized uptake values; SD, standard deviation; MIP, maximum intensity projection; ANOVA, analysis of variance; $CuSO_4$, copper sulfate; ROIs, regions of interest; TACs, time activity curves; Na_2SO_4, sodium sulfate; NH_4Cl, ammonium chloride; Et_2O, diethyl ether; K_2CO_3, potassium carbonate; NaOH, sodium hydroxide; HCl, hydrochloric acid; SDS, sodium dodecyl sulfate; FBS, fetal bovine serum; DMEM, Dulbecco's modified Eagle's medium; BCA, bicinchoninic acid; bs, broad signal; CDCl3, deuterated chloroform; $K_{2.2.2}$, Kryptofix 2.2.2; Boc, *tert*-butoxycarbonyl;

References

1. McConathy, J.; Yu, W.; Jarkas, N.; Seo, W.; Schuster, D. M.; Goodman, M. M. Radiohalogenated nonnatural amino acids as PET and SPECT tumor imaging agents. *Med. Res. Rev.* **2012,** *32*, 868-905.

2. Sai, K. K.; Huang, C.; Yuan, L.; Zhou, D.; Piwnica-Worms, D.; Garbow, J. R.; Engelbach, J. A.; Mach, R. H.; Rich, K. M.; McConathy, J. ^{18}F-AFETP, ^{18}F-FET, and ^{18}F-FDG imaging of mouse DBT gliomas. *J. Nucl. Med.* **2013,** *54*, 1120-1126.

3. McConathy, J.; Goodman, M. M. Non-natural amino acids for tumor imaging using positron emission tomography and single photon emission computed tomography. *Cancer Metastasis Rev.* **2008,** *27*, 555-573.

4. Huang, C.; McConathy, J. Fluorine-18 labeled amino acids for oncologic imaging with positron emission tomography. *Curr. Top. Med. Chem.* **2013,** *13*, 871-891.

5. Pauleit, D.; Stoffels, G.; Bachofner, A.; Floeth, F. W.; Sabel, M.; Herzog, H.; Tellmann, L.; Jansen, P.; Reifenberger, G.; Hamacher, K.; Coenen, H. H.; Langen, K. J. Comparison of ^{18}F-FET and ^{18}F-FDG PET in brain tumors. *Nucl. Med. Biol.* **2009,** *36*, 779-787.

6. Chen, W.; Silverman, D. H. S.; Delaloye, S.; Czernin, J.; Kamdar, N.; Pope, W.; Satyamurthy, N.; Schiepers, C.; Cloughesy, T. ^{18}F-FDOPA PET imaging of brain tumors: Comparison study with ^{18}F-FDG PET and evaluation of diagnostic accuracy. *J. Nucl. Med.* **2006,** *47*, 904-911.

7. Popperl, G.; Kreth, F. W.; Mehrkens, J. H.; Herms, J.; Seelos, K.; Koch, W.; Gildehaus, F. J.; Kretzschmar, H. A.; Tonn, J. C.; Tatsch, K. FET PET for the evaluation of untreated gliomas: Correlation of FET uptake and uptake kinetics with tumour grading. *Eur. J .Nucl. Med. Mol. Imaging* **2007,** *34*, 1933-1942.

8. Floeth, F. W.; Pauleit, D.; Sabel, M.; Stoffels, G.; Reifenberger, G.; Riemenschneider, M. J.; Jansen, P.; Coenen, H. H.; Steiger, H. J.; Langen, K. J. Prognostic value of *O*-(2-^{18}F-fluoroethyl)-L-tyrosine PET and MRI in low-grade glioma. *J. Nucl. Med.* **2007,** *48*, 519-527.

9. Langen, K. J.; Hamacher, K.; Weckesser, M.; Floeth, F.; Stoffels, G.; Bauer, D.; Coenen, H. H.; Pauleit, D. *O*-(2-[^{18}F]Fluoroethyl)-L-tyrosine: Uptake mechanisms and clinical applications. *Nucl. Med. Biol.* **2006,** *33*, 287-294.

10. Weckesser, M.; Langen, K. J.; Rickert, C. H.; Kloska, S.; Straeter, R.; Hamacher, K.; Kurlemann, G.; Wassmann, H.; Coenen, H. H.; Schober, O. *O*-(2-[^{18}F]Fluorethyl)-L-tyrosine PET in the clinical evaluation of primary brain tumours. *Eur. J .Nucl. Med. Mol. Imaging* **2005,** *32*, 422-429.

11. Tripathi, M.; Sharma, R.; D'Souza, M.; Jaimini, A.; Panwar, P.; Varshney, R.; Datta, A.; Kumar, N.; Garg, G.; Singh, D.; Grover, R. K.; Mishra, A. K.; Mondal, A. Comparative evaluation of F-18 FDOPA, F-18 FDG, and F-18 FLT-PET/CT for metabolic imaging of low grade gliomas. *Clin. Nucl. Med.* **2009,** *34*, 878-883.

12. Seibyl, J. P.; Chen, W.; Silverman, D. H. S. 3,4-Dihydroxy-6-[^{18}F]-fluoro-L-phenylalanine positron emission tomography in patients with central motor disorders and in evaluation of brain and other tumors. *Semin. Nucl. Med.* **2007,** *37*, 440-450.

13. Schuster, D. M.; Savir-Baruch, B.; Nieh, P. T.; Master, V. A.; Halkar, R. K.; Rossi, P. J.; Lewis, M. M.; Nye, J. A.; Yu, W.; Bowman, F. D.; Goodman, M. M. Detection of recurrent prostate carcinoma with anti-1-amino-3-^{18}F-fluorocyclobutane-1-carboxylic acid PET/CT and ^{111}In-capromab pendetide SPECT/CT. *Radiology* **2011,** *259*, 852-861.

14. Schuster, D. M.; Votaw, J. R.; Nieh, P. T.; Yu, W.; Nye, J. A.; Master, V.; Bowman, F. D.; Issa, M. M.; Goodman, M. M. Initial experience with the radiotracer *anti*-1-amino-3-^{18}F-fluorocyclobutane-1-carboxylic acid with PET/CT in prostate carcinoma. *J. Nucl. Med.* **2007,** *48*, 56-63.

15. Montravers, F.; Grahek, D.; Kerrou, K.; Ruszniewski, P.; de Beco, V.; Aide, N.; Gutman, F.; Grange, J. D.; Lotz, J. P.; Talbot, J. N. Can fluorodihydroxyphenylalanine PET replace somatostatin receptor scintigraphy in patients with digestive endocrine tumors? *J. Nucl. Med.* **2006,** *47*, 1455-1462.

16. Becherer, A.; Szabo, M.; Karanikas, G.; Wunderbaldinger, P.; Angelberger, P.; Raderer, M.; Kurtaran, A.; Dudczak, R.; Kletter, K. Imaging of advanced neuroendocrine tumors with ^{18}F-FDOPA PET. *J. Nucl. Med.* **2004,** *45*, 1161-1167.

17. Jager, P. L.; Chirakal, R.; Marriott, C. J.; Brouwers, A. H.; Koopmans, K. P.; Gulenchyn, K. Y. 6-L-^{18}F-Fluorodihydroxyphenylalanine PET in neuroendocrine tumors: Basic aspects and emerging clinical applications. *J. Nucl. Med.* **2008,** *49*, 573-586.

18. Ono, M.; Oka, S.; Okudaira, H.; Schuster, D. M.; Goodman, M. M.; Kawai, K.; Shirakami, Y. Comparative evaluation of transport mechanisms of *trans*-1-amino-3-[^{18}F]fluorocyclobutanecarboxylic acid and L-[methyl-^{11}C]methionine in human glioma cell lines. *Brain Res.* **2013,** *1535*, 24-37.

19. Oka, S.; Okudaira, H.; Ono, M.; Schuster, D. M.; Goodman, M. M.; Kawai, K.; Shirakami, Y. Differences in transport mechanisms of *trans*-1-amino-3-[^{18}F]fluorocyclobutanecarboxylic acid in inflammation, prostate cancer, and glioma cells: Comparison with L-[methyl-^{11}C]methionine and 2-deoxy-2-[^{18}F]fluoro-D-glucose. *Mol. Imaging Biol.* **2014,** *16*, 322-329.

20. Schuster, D. M.; Taleghani, P. A.; Nieh, P. T.; Master, V. A.; Amzat, R.; Savir-Baruch, B.; Halkar, R. K.; Fox, T.; Osunkoya, A. O.; Moreno, C. S.; Nye, J. A.; Yu, W.; Fei, B.; Wang, Z.; Chen, Z.; Goodman, M. M. Characterization of primary prostate carcinoma by *anti*-1-amino-2-[^{18}F]fluorocyclobutane-1-carboxylic acid (*anti*-3-[^{18}F]FACBC) uptake. *Am. J. Nucl. Med. Mol. Imaging* **2013,** *3*, 85-96.

21. Shoup, T. M.; Olson, J.; Hoffman, J. M.; Votaw, J.; Eshima, D.; Eshima, L.; Camp, V. M.; Stabin, M.; Votaw, D.; Goodman, M. M. Synthesis and evaluation of [^{18}F]1-amino-3-fluorocyclobutane-1-carboxylic acid to image brain tumors. *J. Nucl. Med.* **1999,** *40*, 331-338.

22. Venneti, S.; Dunphy, M. P.; Zhang, H.; Pitter, K. L.; Zanzonico, P.; Campos, C.; Carlin, S. D.; La Rocca, G.; Lyashchenko, S.; Ploessl, K.; Rohle, D.; Omuro, A. M.; Cross, J. R.; Brennan, C. W.; Weber, W. A.; Holland, E. C.; Mellinghoff, I. K.; Kung, H. F.; Lewis, J. S.; Thompson, C. B. Glutamine-based PET imaging facilitates enhanced metabolic evaluation of gliomas in vivo. *Sci. Transl. Med.* **2015,** *7*, 274ra217.

23. Qu, W.; Zha, Z.; Ploessl, K.; Lieberman, B. P.; Zhu, L.; Wise, D. R.; Thompson, C. B.; Kung, H. F. Synthesis of optically pure 4-fluoro-glutamines as potential metabolic imaging agents for tumors. *J. Am. Chem. Soc.* **2011,** *133*, 1122-1133.

24. Lieberman, B. P.; Ploessl, K.; Wang, L.; Qu, W.; Zha, Z.; Wise, D. R.; Chodosh, L. A.; Belka, G.; Thompson, C. B.; Kung, H. F. PET imaging of glutaminolysis in tumors by ^{18}F-(2*S*,4*R*)4-fluoroglutamine. *J. Nucl. Med.* **2011,** *52*, 1947-1955.

25. Wang, L.; Zha, Z.; Qu, W.; Qiao, H.; Lieberman, B. P.; Plossl, K.; Kung, H. F. Synthesis and evaluation of ^{18}F-labeled alanine derivatives as potential tumor imaging agents. *Nucl. Med. Biol.* **2012,** *39*, 933-943.

26. Baek, S.; Mueller, A.; Lim, Y. S.; Lee, H. C.; Lee, Y. J.; Gong, G.; Kim, J. S.; Ryu, J. S.; Oh, S. J.; Lee, S. J.; Bacher-Stier, C.; Fels, L.; Koglin, N.; Schatz, C. A.; Dinkelborg, L. M.; Moon, D. H. (4*S*)-4-(3-[^{18}F]Fluoropropyl)-L-glutamate for imaging of x_C^- transporter activity in hepatocellular carcinoma using PET: preclinical and exploratory clinical studies. *J. Nucl. Med.* **2013,** *54*, 117-123.

27. Baek, S.; Choi, C. M.; Ahn, S. H.; Lee, J. W.; Gong, G.; Ryu, J. S.; Oh, S. J.; Bacher-Stier, C.; Fels, L.; Koglin, N.; Hultsch, C.; Schatz, C. A.; Dinkelborg, L. M.; Mittra, E. S.; Gambhir, S. S.; Moon, D. H. Exploratory clinical trial of (4*S*)-4-(3-[^{18}F]fluoropropyl)-L-glutamate for imaging x_C^- transporter using positron emission tomography in patients with non-small cell lung or breast cancer. *Clin. Cancer Res.* **2012,** *18*, 5427-5437.

28. Koglin, N.; Mueller, A.; Berndt, M.; Schmitt-Willich, H.; Toschi, L.; Stephens, A. W.; Gekeler, V.; Friebe, M.; Dinkelborg, L. M. Specific PET imaging of x_C^- transporter activity using a ^{18}F-labeled glutamate derivative reveals a dominant pathway in tumor metabolism. *Clin. Cancer Res.* **2011,** *17*, 6000-6011.

29. McConathy, J.; Zhou, D.; Shockley, S. E.; Jones, L. A.; Griffin, E. A.; Lee, H.; Adams, S. J.; Mach, R. H. Click synthesis and biologic evaluation of (*R*)- and (*S*)-2-amino-3-[1-(2-[^{18}F]fluoroethyl)-1*H*-[1,2,3]triazol-4-yl]propanoic acid for brain tumor imaging with positron emission tomography. *Mol. Imaging* **2010,** *9*, 329-342.

30. Muller, A.; Chiotellis, A.; Keller, C.; Ametamey, S. M.; Schibli, R.; Mu, L.; Kramer, S. D. Imaging tumour ATB0,+ transport activity by PET with the cationic amino acid *O*-2((2-[^{18}F]fluoroethyl)methyl-amino)ethyltyrosine. *Mol. Imaging Biol.* **2014,** *16*, 412-420.

31. Yu, W.; McConathy, J.; Williams, L.; Camp, V. M.; Malveaux, E. J.; Zhang, Z.; Olson, J. J.; Goodman, M. M. Synthesis, radiolabeling, and biological evaluation of (*R*)- and (*S*)-2-amino-3-[^{18}F]fluoro-2-methylpropanoic acid (FAMP) and (*R*)- and (*S*)-3-[^{18}F]fluoro-2-methyl-2-*N*-(methylamino)propanoic acid (*N*MeFAMP) as potential PET radioligands for imaging brain tumors. *J. Med. Chem.* **2010,** *53*, 876-886.

32. McConathy, J.; Martarello, L.; Malveaux, E. J.; Camp, V. M.; Simpson, N. E.; Simpson, C. P.; Bowers, G. D.; Zhang, Z.; Olson, J. J.; Goodman, M. M. Synthesis and evaluation of 2-amino-4-[^{18}F]fluoro-2-methylbutanoic acid (FAMB): Relationship of amino acid transport to tumor imaging properties of branched fluorinated amino acids. *Nucl. Med. Biol.* **2003,** *30*, 477-490.

33. McConathy, J.; Martarello, L.; Malveaux, E. J.; Camp, V. M.; Simpson, N. E.; Simpson, C. P.; Bowers, G. D.; Olson, J. J.; Goodman, M. M. Radiolabeled amino acids for tumor imaging with PET: Radiosynthesis and biological evaluation of 2-amino-3-[^{18}F]fluoro-2-methylpropanoic acid and 3-[^{18}F]fluoro-2-methyl-2-(methylamino)propanoic acid. *J. Med. Chem.* **2002,** *45*, 2240-2249.

34. Jost, S. C.; Wanebo, J. E.; Song, S. K.; Chicoine, M. R.; Rich, K. M.; Woolsey, T. A.; Lewis, J. S.; Mach, R. H.; Xu, J.; Garbow, J. R. In vivo imaging in a murine model of glioblastoma. *Neurosurgery* **2007,** *60*, 360-370; discussion 370-361.

35. Charrier, J. D.; Hadfield, D. S.; Hitchcock, P. B.; Young, D. W. Synthesis of (2*S*,4*S*)- and (2*S*,4*R*)-5-fluoroleucine and (2*S*,4*S*)-[5,5-$^{2}H_2$]-5-fluoroleucine. *Org. Biomol. Chem.* **2004,** *2*, 474-482.

36. Kim, D. W.; Jeong, H. J.; Lim, S. T.; Sohn, M. H.; Katzenellenbogen, J. A.; Chi, D. Y. Facile nucleophilic fluorination reactions using *tert*-alcohols as a reaction medium: Significantly enhanced reactivity of alkali metal fluorides and improved selectivity. *J. Org. Chem.* **2008,** *73*, 957-962.

37. Yu, W.; McConathy, J.; Olson, J. J.; Goodman, M. M. System A amino acid transport-targeted brain and systemic tumor PET imaging agents 2-amino-3-[^{18}F]fluoro-2-methylpropanoic acid and 3-[^{18}F]fluoro-2-methyl-2-(methylamino)propanoic acid. *Nucl. Med. Biol.* **2015,** *42*, 8-18.

38. Ploessl, K.; Wang, L.; Lieberman, B. P.; Qu, W.; Kung, H. F. Comparative evaluation of 18F-labeled glutamic acid and glutamine as tumor metabolic imaging agents. *J. Nucl. Med.* **2012,** *53*, 1616-1624.

39. Goberdhan, D. C.; Ogmundsdottir, M. H.; Kazi, S.; Reynolds, B.; Visvalingam, S. M.; Wilson, C.; Boyd, C. A. Amino acid sensing and mTOR regulation: Inside or out? *Biochem. Soc. Trans.* **2009,** *37*, 248-252.

40. Beugnet, A.; Tee, A. R.; Taylor, P. M.; Proud, C. G. Regulation of targets of mTOR (mammalian target of rapamycin) signalling by intracellular amino acid availability. *Biochem. J.* **2003,** *372*, 555-566.

41. Fuchs, B. C.; Finger, R. E.; Onan, M. C.; Bode, B. P. ASCT2 silencing regulates mammalian target-of-rapamycin growth and survival signaling in human hepatoma cells. *Am. J. Physiol. Cell Physiol.* **2007,** *293*, C55-63.

42. Fuchs, B. C.; Bode, B. P. Amino acid transporters ASCT2 and LAT1 in cancer: Partners in crime? *Semin. Cancer Biol.* **2005,** *15*, 254-266.

43. Hyde, R.; Hajduch, E.; Powell, D. J.; Taylor, P. M.; Hundal, H. S. Ceramide down-regulates System A amino acid transport and protein synthesis in rat skeletal muscle cells. *FASEB J.* **2005,** *19*, 461-463.

44. Barrow, J. C.; Coburn, C. A.; Mcgaughey, G. B.; Nantermet, P. G.; Rajapakse, H. A.; Selnick, H. G.; Stachel, S. J.; Stanton, M. G.; Stauffer, S. R.; Vacca, J. P. 2, 4, 6-Substituted pyridyl derivative compounds useful as beta-secretase inhibitors for the treatment of Alzheimer's disease. WO2005103043 A1, **2005**.

45. Wang, X.; Yin, L.; Yang, T.; Wang, Y. M. Synthesis of new dimeric-PEG-supported cinchona ammonium salts as chiral phase transfer catalysts for the alkylation of Schiff bases with water as the solvent. *Tetrahedron: Asymmetry* **2007,** *18*, 108-114.

46. Laue, K. W.; Muck-Lichtenfeld, C.; Haufe, G. Enantioselective syntheses of 2-amino-4-fluoropent-4-enoic acids. Isosteres of asparagine. *Tetrahedron* **1999,** *55*, 10413-10424.

47. Hamed, R. B.; Henry, L.; Gomez-Castellanos, J. R.; Mecinovic, J.; Ducho, C.; Sorensen, J. L.; Claridge, T. D.; Schofield, C. J. Crotonase catalysis enables flexible production of functionalized prolines and carbapenams. *J. Am. Chem. Soc.* **2012,** *134*, 471-479.

48. Pattarozzi, M.; Zonta, C.; Broxterman, Q. B.; Kaptein, B.; De Zorzi, R.; Randaccio, L.; Scrimin, P.; Licini, G. Stereoselective iodocyclization of (*S*)-allylalanine derivatives: γ-Lactone vs cyclic carbamate formation. *Org. Lett.* **2007,** *9*, 2365-2368.

49. Zuhayra, M.; Alfteimi, A.; Von Forstner, C.; Lutzen, U.; Meller, B.; Henze, E. New approach for the synthesis of [^{18}F]fluoroethyltyrosine for cancer imaging: Simple, fast, and high yielding automated synthesis. *Bioorg. Med. Chem.* **2009,** *17*, 7441-7448.

50. Jost, S. C.; Collins, L.; Travers, S.; Piwnica-Worms, D.; Garbow, J. R. Measuring brain tumor growth: Combined bioluminescence imaging-magnetic resonance imaging strategy. *Mol. Imaging* **2009,** *8*, 245-253.

Table of Contents Graphic